Cavenee. 1989. Mitotic recombination of chromosome 17 in astrocytomas. Proc. Natl. Acad. Sci. USA **86**:2858–2862.
41. **Jinks-Robertson, S., M. Michelitch, and S. Ramcharan.** 1993. Substrate length requirements for efficient mitotic recombination in *Saccharomyces cerevisiae*. Mol. Cell. Biol. **13**:3937–3950.
42. **Johnson, R. D., and M. Jasin.** 2000. Sister chromatid gene conversion is a prominent double-strand break repair pathway in mammalian cells. EMBO J. **19**:3398–3407.
43. **Klinedinst, D. K., and N. R. Drinkwater.** 1991. Reduction to homozygosity is the predominant spontaneous mutational event in cultured human lymphoblastoid cells. Mutat. Res. **250**:365–374.
44. **Kobayashi, I., and H. Ikeda.** 1983. Double Holliday structure: a possible in vivo intermediate form of general recombination in Escherichia coli. Mol. Gen. Genet. **191**:213–220.
45. **Kraus, E., W. Y. Leung, and J. E. Haber.** 2001. Break-induced replication: a review and an example in budding yeast. Proc. Natl. Acad. Sci. USA **98**: 8255–8262.
46. **Lander, E. S., L. M. Linton, B. Birren, C. Nusbaum, M. C. Zody, J. Baldwin, K. Devon, K. Dewar, M. Doyle, W. FitzHugh, R. Funke, D. Gage, K. Harris, A. Heaford, J. Howland, L. Kann, J. Lehoczky, R. LeVine, P. McEwan, K. McKernan, J. Meldrim, J. P. Mesirov, C. Miranda, W. Morris, J. Naylor, C. Raymond, M. Rosetti, R. Santos, A. Sheridan, C. Sougnez, N. Stange-Thomann, N. Stojanovic, A. Subramanian, D. Wyman, J. Rogers, J. Sulston, R. Ainscough, S. Beck, D. Bentley, J. Burton, C. Clee, N. Carter, A. Coulson, R. Deadman, P. Deloukas, A. Dunham, I. Dunham, R. Durbin, L. French, D. Grafham, S. Gregory, T. Hubbard, S. Humphray, A. Hunt, M. Jones, C. Lloyd, A. McMurray, L. Matthews, S. Mercer, S. Milne, J. C. Mullikin, A. Mungall, R. Plumb, M. Ross, R. Shownkeen, S. Sims, R. H. Waterston, R. K. Wilson, L. W. Hillier, J. D. McPherson, M. A. Marra, E. R. Mardis, L. A. Fulton, A. T. Chinwalla, K. H. Pepin, W. R. Gish, S. L. Chissoe, M. C. Wendl, K. D. Delehaunty, T. L. Miner, A. Delehaunty, J. B. Kramer, L. L. Cook, R. S. Fulton, D. L. Johnson, P. J. Minx, S. W. Clifton, T. Hawkins, E. Branscomb, P. Predki, P. Richardson, S. Wenning, T. Slezak, N. Doggett, J. F. Cheng, A. Olsen, S. Lucas, C. Elkin, E. Uberbacher, M. Frazier, et al.** 2001. Initial sequencing and analysis of the human genome. Nature **409**:860–921.
47. **Li, C. Y., D. W. Yandell, and J. B. Little.** 1992. Molecular mechanisms of spontaneous and induced loss of heterozygosity in human cells in vitro. Somat. Cell Mol. Genet. **18**:77–87.
48. **Li, J., L. R. Read, and M. D. Baker.** 2001. The mechanism of mammalian gene replacement is consistent with the formation of long regions of heteroduplex DNA associated with two crossing-over events. Mol. Cell. Biol. **21**: 501–510.
49. **Liang, L., L. Deng, C. Shao, P. J. Stambrook, and J. A. Tischfield.** 2000. In vivo loss of heterozygosity in T-cells of B6C3F1 Aprt(+/−) mice. Environ. Mol. Mutagen. **35**:150–157.
50. **Liber, H. L., and W. G. Thilly.** 1982. Mutation assay at the thymidine kinase locus in diploid human lymphoblasts. Mutat. Res. **94**:467–485.
51. **Liskay, R. M., and J. L. Stachelek.** 1983. Evidence for intrachromosomal gene conversion in cultured mouse cells. Cell **35**:157–165.
52. **Liskay, R. M., and J. L. Stachelek.** 1986. Information transfer between duplicated chromosomal sequences in mammalian cells involves contiguous regions of DNA. Proc. Natl. Acad. Sci. USA **83**:1802–1806.
53. **Lo, Y. C., K. S. Paffett, O. Amit, J. A. Clikeman, R. Sterk, M. A. Brenneman, and J. A. Nickoloff.** 2006. Sgs1 regulates gene conversion tract lengths and crossovers independently of its helicase activity. Mol. Cell. Biol. **26**:4086–4094.
54. **Malkova, A., E. L. Ivanov, and J. E. Haber.** 1996. Double-strand break repair in the absence of RAD51 in yeast: a possible role for break-induced DNA replication. Proc. Natl. Acad. Sci. USA **93**:7131–7136.
55. **Maloisel, L., J. Bhargava, and G. S. Roeder.** 2004. A role for DNA polymerase delta in gene conversion and crossing over during meiosis in Saccharomyces cerevisiae. Genetics **167**:1133–1142.
56. **McEachern, M. J., and J. E. Haber.** 2006. Break-induced replication and recombinational telomere elongation in yeast. Annu. Rev. Biochem. **75**:111–135.
57. **McGill, C. B., B. K. Shafer, L. K. Derr, and J. N. Strathern.** 1993. Recombination initiated by double-strand breaks. Curr. Genet. **23**:305–314.
58. **Meselson, M. S., and C. M. Radding.** 1975. A general model for genetic recombination. Proc. Natl. Acad. Sci. USA **72**:358–361.
59. **Miller, E. M., H. L. Hough, J. W. Cho, and J. A. Nickoloff.** 1997. Mismatch repair by efficient nick-directed, and less efficient mismatch-specific, mechanisms in homologous recombination intermediates in Chinese hamster ovary cells. Genetics **147**:743–753.
60. **Morley, A. A.** 1991. Mitotic recombination in mammalian cells in vivo. Mutat. Res. **250**:345–349.
61. **Morley, A. A., S. A. Grist, D. R. Turner, A. Kutlaca, and G. Bennett.** 1990. Molecular nature of in vivo mutations in human cells at the autosomal HLA-A locus. Cancer Res **50**:4584–4587.
62. **Moynahan, M. E., and M. Jasin.** 1997. Loss of heterozygosity induced by a chromosomal double-strand break. Proc. Natl. Acad. Sci. USA **94**:8988–8993.
63. **Nassif, N., J. Penney, S. Pal, W. R. Engels, and G. B. Gloor.** 1994. Efficient copying of nonhomologous sequences from ectopic sites via P-element-induced gap repair. Mol. Cell. Biol. **14**:1613–1625.
64. **Nickoloff, J. A., D. B. Sweetser, J. A. Clikeman, G. J. Khalsa, and S. L. Wheeler.** 1999. Multiple heterologies increase mitotic double-strand break-induced allelic gene conversion tract lengths in yeast. Genetics **153**:665–679.
65. **Paques, F., and J. E. Haber.** 1999. Multiple pathways of recombination induced by double-strand breaks in *Saccharomyces cerevisiae*. Microbiol. Mol. Biol. Rev. **63**:349–404.
66. **Prado, F., and A. Aguilera.** 2003. Control of cross-over by single-strand DNA resection. Trends Genet. **19**:428–431.
67. **Quintana, P. J., E. A. Neuwirth, and A. J. Grosovsky.** 2001. Interchromosomal gene conversion at an endogenous human cell locus. Genetics **158**: 757–767.
68. **Raghavan, M., D. M. Lillington, S. Skoulakis, S. Debernardi, T. Chaplin, N. J. Foot, T. A. Lister, and B. D. Young.** 2005. Genome-wide single nucleotide polymorphism analysis reveals frequent partial uniparental disomy due to somatic recombination in acute myeloid leukemias. Cancer Res **65**:375–378.
69. **Richardson, C., and M. Jasin.** 2000. Coupled homologous and nonhomologous repair of a double-strand break preserves genomic integrity in mammalian cells. Mol. Cell. Biol. **20**:9068–9075.
70. **Richardson, C., and M. Jasin.** 2000. Frequent chromosomal translocations induced by DNA double-strand breaks. Nature **405**:697–700.
71. **Richardson, C., M. E. Moynahan, and M. Jasin.** 1998. Double-strand break repair by interchromosomal recombination: suppression of chromosomal translocations. Genes Dev. **12**:3831–3842.
72. **Richardson, C., J. M. Stark, M. Ommundsen, and M. Jasin.** 2004. Rad51 overexpression promotes alternative double-strand break repair pathways and genome instability. Oncogene **23**:546–553.
73. **Roman, H.** 1980. Recombination in diploid vegetative cells of Saccharomyces cerevisiae. Carlsberg Res. Commun. **45**:211–224.
74. **Rong, Y. S., and K. G. Golic.** 2003. The homologous chromosome is an effective template for the repair of mitotic DNA double-strand breaks in Drosophila. Genetics **165**:1831–1842.
75. **Sargent, R. G., M. A. Brenneman, and J. H. Wilson.** 1997. Repair of site-specific double-strand breaks in a mammalian chromosome by homologous and illegitimate recombination. Mol. Cell. Biol. **17**:267–277.
76. **Schwacha, A., and N. Kleckner.** 1995. Identification of double Holliday junctions as intermediates in meiotic recombination. Cell **83**:783–791.
77. **Schwacha, A., and N. Kleckner.** 1994. Identification of joint molecules that form frequently between homologs but rarely between sister chromatids during yeast meiosis. Cell **76**:51–63.
78. **Shao, C., L. Deng, O. Henegariu, L. Liang, N. Raikwar, A. Sahota, P. J. Stambrook, and J. A. Tischfield.** 1999. Mitotic recombination produces the majority of recessive fibroblast variants in heterozygous mice. Proc. Natl. Acad. Sci. USA **96**:9230–9235.
79. **Sharples, G. J.** 2001. The X philes: structure-specific endonucleases that resolve Holliday junctions. Mol. Microbiol. **39**:823–834.
80. **Shulman, M. J., C. Collins, A. Connor, L. R. Read, and M. D. Baker.** 1995. Interchromosomal recombination is suppressed in mammalian somatic cells. EMBO J. **14**:4102–4107.
81. **Sigal, N., and B. Alberts.** 1972. Genetic recombination: the nature of a crossed strand-exchange between two homologous DNA molecules. J. Mol. Biol. **71**:789–793.
82. **Skopek, T. R., H. L. Liber, B. W. Penman, and W. G. Thilly.** 1978. Isolation of a human lymphoblastoid line heterozygous at the thymidine kinase locus: possibility for a rapid human cell mutation assay. Biochem. Biophys. Res. Commun. **84**:411–416.
83. **Stark, J. M., and M. Jasin.** 2003. Extensive loss of heterozygosity is suppressed during homologous repair of chromosomal breaks. Mol. Cell. Biol. **23**:733–743.
84. **Sun, H., D. Dawson, and J. W. Szostak.** 1991. Genetic and physical analyses of sister chromatid exchange in yeast meiosis. Mol. Cell. Biol. **11**:6328–6336.
85. **Symington, L. S., L. E. Kang, and S. Moreau.** 2000. Alteration of gene conversion tract length and associated crossing over during plasmid gap repair in nuclease-deficient strains of Saccharomyces cerevisiae. Nucleic Acids Res. **28**:4649–4656.
86. **Szostak, J. W., T. L. Orr-Weaver, R. J. Rothstein, and F. W. Stahl.** 1983. The double-strand-break repair model for recombination. Cell **33**:25–35.
87. **Taghian, D. G., and J. A. Nickoloff.** 1997. Chromosomal double-strand breaks induce gene conversion at high frequency in mammalian cells. Mol. Cell. Biol. **17**:6386–6393.
88. **Tanaka, K., K. Watanabe, M. Mori, H. Kamisaku, H. Tsuji, Y. Hirabayashi, T. Inoue, K. Yoshida, and S. Aizawa.** 2002. Cytogenetic and cellular events during radiation-induced thymic lymphomagenesis in the p53 heterozygous (+/−) B10 mouse. Int. J. Radiat. Biol. **78**:165–172.
89. **Tch, M. T., D. Blaydon, T. Chaplin, N. J. Foot, S. Skoulakis, M. Raghavan, C. A. Harwood, C. M. Proby, M. P. Philpott, B. D. Young, and D. P. Kelsell.** 2005. Genomewide single nucleotide polymorphism microarray mapping in basal cell carcinomas unveils uniparental disomy as a key somatic event. Cancer Res. **65**:8597–8603.

90. **Thomas, K. R., and M. R. Capecchi.** 1987. Site-directed mutagenesis by gene targeting in mouse embryo-derived stem cells. Cell **51**:503–512.
91. **Tischfield, J. A.** 1997. Loss of heterozygosity or: how I learned to stop worrying and love mitotic recombination. Am. J. Hum. Genet. **61**:995–999.
92. **Van Sloun, P. P., S. W. Wijnhoven, H. J. Kool, R. Slater, G. Weeda, A. A. van Zeeland, P. H. Lohman, and H. Vrieling.** 1998. Determination of spontaneous loss of heterozygosity mutations in Aprt heterozygous mice. Nucleic Acids Res. **26**:4888–4894.
93. **Weinstock, D. M., C. A. Richardson, B. Elliott, and M. Jasin.** 2006. Modeling oncogenic translocations: distinct roles for double-strand break repair pathways in translocation formation in mammalian cells. DNA Repair (Amsterdam) **5**:1065–1074.
94. **Wolff, S.** 1977. Sister chromatid exchange. Annu. Rev. Genet. **11**:183–201.
95. **Wu, L., and I. D. Hickson.** 2003. The Bloom's syndrome helicase suppresses crossing over during homologous recombination. Nature **426**:870–874.

Available online at www.sciencedirect.com
ScienceDirect
Mutation Research 625 (2007) 83–93
Fundamental and Molecular Mechanisms of Mutagenesis
www.elsevier.com/locate/molmut
Community address: www.elsevier.com/locate/mutres

Application of the adductome approach to assess intertissue DNA damage variations in human lung and esophagus

Robert A. Kanaly [a,b], Saburo Matsui [a], Tomoyuki Hanaoka [c], Tomonari Matsuda [a,*]

[a] *Department of Technology and Ecology, Graduate School of Global Environmental Studies, Kyoto University, Kyoto 606-8501, Japan*
[b] *Department of Environmental Biosciences, International Graduate School of Arts and Sciences, Yokohama City University, Yokohama 236-0027, Japan*
[c] *Epidemiology and Prevention Division, National Cancer Center Research Institute, Tokyo 104-0045, Japan*

Received 28 February 2007; received in revised form 9 May 2007; accepted 14 May 2007
Available online 21 May 2007

Abstract

Methods for determining the differential susceptibility of human organs to DNA damage have not yet been explored to any large extent due to technical constraints. The development of comprehensive analytical approaches by which to detect intertissue variations in DNA damage susceptibility may advance our understanding of the roles of DNA adducts in cancer etiology and as exposure biomarkers at least. A strategy designed for the detection and comparison of multiple DNA adducts from different tissue samples was applied to assess esophageal and peripherally- and centrally-located lung tissue DNA obtained from the same person. This adductome approach utilized LC/ESI-MS/MS analysis methods designed to detect the neutral loss of 2′-deoxyribose from positively ionized 2′-deoxynucleoside adducts transmitting the $[M+H]^+ > [M+H-116]^+$ transition over 374 transitions. In the final analyses, adductome maps were produced which facilitated the visualization of putative DNA adducts and their relative levels of occurrence and allowed for comprehensive comparisons between samples, including a calf thymus DNA negative control. The largest putative adducts were distributed similarly across the samples, however, differences in the relative amounts of putative adducts in lung and esophagus tissue were also revealed. The largest-occurring lung tissue DNA putative adducts were 90% similar ($n = 50$), while putative adducts in esophagus tissue DNA were shown to be 80 and 84% similar to central and peripheral lung tissue DNA respectively. Seven DNA adducts, N^2-ethyl-2′-deoxyguanosine (N^2-ethyl-dG), 1,N^6-etheno-2′-deoxyadenosine (εdA), α-*S*- and α-*R*-methyl-γ-hydroxy-1,N^2-propano-2′-deoxyguanosine (1,N^2-PdG_1, 1,N^2-PdG_2), 3-(2′-deoxyribosyl)-5,6,7,8-tetrahydro-8-hydroxy-pyrimido[1,2-*a*]purine-(3*H*)-one (8-OH-PdG) and the two stereoisomers of 3-(2′-deoxyribosyl)-5,6,7,8-tetrahydro-6-hydroxypyrimido[1,2-*a*]purine-(3*H*)-one (6-OH-PdG) were unambiguously detected in all tissue DNA samples by comparison to authentic adduct standards and stable isotope dilution and their identities were matched to putative adducts detected in the adductome maps.

Keywords: DNA adduct; Intertissue variation; Adductome; Stable isotope dilution; Esophagus; Lung

1. Introduction

Xenobiotics from the environment and endogenously-produced oxidants may damage DNA by the production of DNA adducts and this vulnerability of cellular DNA to modification occurs continuously [1,2]. Consid-

* Corresponding author. Tel.: +81 75 753 5171; fax: +81 75 753 3335.
E-mail address: matsuda@z05.mbox.media.kyoto-u.ac.jp (T. Matsuda).

0027-5107/$ – see front matter © 2007 Elsevier B.V. All rights reserved.
doi:10.1016/j.mrfmmm.2007.05.006

ering that the initiating event in chemical carcinogenesis is the binding of a reactive compound to DNA to form a DNA adduct, DNA adducts have become the focus of intensive research over the last 30 years and are the subject of recent excellent reviews [3–8]. Generally, DNA adducts are repaired with high efficiency in the cells of the body, however, when adducts are unrepaired or misrepaired they may result in a variety of potentially deleterious consequences such as mutagenesis, carcinogenesis, accelerated aging or neurological syndromes such as Alzheimer's disease. To understand more clearly the roles of DNA adducts in (1) the etiology of these processes, (2) as biomarkers of exposure and (3) as potential markers of cancer risk – as has been called for recently [9–11] – are matters of much interest and the development of new methods to monitor adducts in human DNA may advance our understanding of these roles.

Liquid chromatography coupled with electrospray ionization tandem mass spectrometry (LC/ESI-MS/MS) is a powerful technique that allows for sensitive DNA adduct detection in the picogram range as low as approximately 1 adduct per to 10^9 bases and through the tandem MS, powerful selectivity options are available by utilizing one stage of mass analysis to preselect an ion of interest and a second stage to analyze the induced fragments. Indeed, the future of LC/ESI-MS/MS as a reliable method for analyzing DNA adducts may have strong potential [12–14]. Exploiting these positive aspects of LC/ESI-MS/MS, various groups have developed methods for measuring different DNA adduct types, from different tissues, and from different organisms [15–19] for example and reviewed in [13]. Additionally, multiple DNA adduct monitoring by LC/ESI-MS/MS or by other techniques has also been conducted in some circumstances and sometimes with the aim to compare correlations between different adduct types and/or tissue types [20–23].

The development of techniques that allow for simultaneous monitoring of multiple types of DNA adducts that are complementary to DNA adduct identification processes shall expand our capabilities to analyze DNA damage across a wide spectrum of potential experimental designs. These may include the examination of differences among individuals based upon variables such as occupational exposure, lifestyle, age, sex and genotype. Specifically, comparisons may be performed by analyzing DNA from the same organs of different individuals for example, or comparisons may be performed by analyzing DNA obtained from different locations within the same tissue, or from among different tissues but from within the same individual for example. Currently, although the number of studies may be limited, examination of intratissue and intertissue variations to DNA damage susceptibility may provide insights on a number of issues related to DNA adduct formation in humans. Examples include the capability to compare the relative repair potential or cell turnover of a specific tissue with adduct formation, or the capability to determine the specific susceptibilities of different tissue types or regions of tissue to specific types of DNA damage. In this report, an assessment of intertissue DNA adduct variation from peripherally- and centrally-located lung tissue and esophagus tissue obtained from the same individual is presented and the potential of the adductome approach [24] is discussed.

2. Materials and methods

2.1. Biochemicals and chemicals

The enzymes micrococcal nuclease (MN) and bovine spleen phosphodiesterase II (SPD) were purchased from Worthington Biochemical Corp., (Lakewood, NJ, USA). Bacterial alkaline phosphatase Type III (*E. coli*) and calf thymus DNA were purchased from Sigma Co., (St. Louis, MO, USA). Acrolein monomer was purchased from Tokyo Chemical Industry Co., Ltd. (TCI, Tokyo, Japan) and [U-$^{15}N_5$]-2′-deoxyguanosine ([U-$^{15}N_5$]-dG, 98% purity) was from Cambridge Isotope Laboratories, Inc., Andover, MA, USA.

Analytical standards of the following DNA adducts, N^2-ethyl-2′-deoxyguanosine (N^2-ethyl-dG), the stereoisomers α-*S*- and α-*R*-methyl-γ-hydroxy-1,N^2-propano-2′-deoxyguanosine (1,N^2-PdG$_1$, 1,N^2-PdG$_2$), 3-(2′-deoxyribosyl)-5,6,7,8-tetrahydro-8-hydroxy-pyrimido[1,2-*a*]purine-(3*H*)-one (8-OH-PdG) and the two stereoisomers 3-(2′-deoxyribosyl)-5,6,7,8-tetrahydro-6-hydroxypyrimido[1,2-*a*]purine-(3*H*)-one (6-OH-PdG) were synthesized as described below, while standards of 1,N^6-etheno-2′-deoxyadenosine (εdA) and dideoxyinosine (ddI) were purchased from Sigma. Acetaldehyde (AA), formaldehyde, *trans*-2-butenal (crotonaldehyde), sodium cyanoborohydride ($NaBH_3CN$), dimethyl sulfoxide (DMSO) and methanol, HPLC grade, were purchased from Wako Chemical (Osaka, Japan).

2.2. Preparation of DNA adduct internal standards

Preparation of 2′-deoxyguanosine-acrolein adducts, 6-OH-PdG and 8-OH-PdG, was carried out by reacting 10 mg of 2′-deoxyguanosine with 6 μl of acrolein in 12 ml of 0.025 M phosphate buffer (pH 7.5). The incubation proceeded for five days in the dark in a 37 °C water bath with reciprocal shaking at 150 rpm. The resulting reaction mixture was subjected to reverse phase column chromatography by application to Sep-Pak C18 cartridges (Waters Corp., Milford, MA, USA) whereby the columns were preconditioned with 10 ml methanol and 5 ml distilled water, and the sample was applied and eluted with approximately 5 ml of methanol. The result-

ing solutions were each concentrated en vacuo, recombined and redissolved in a total of 600 μl of DMSO. Fifty microliter aliquots of sample were subjected to preparative HPLC using a Shimadzu LC10-ATVP model pump (Shimadzu, Kyoto, Japan) equipped with a Rheodyne model 7725i injector (Rheodyne, Cotati, CA, USA) and a C18 reverse phase column (Shim-pack FC-ODS, 150 mm × 4.6 mm, Shimadzu) and the fractions were collected. The mobile phase consisted of a water and methanol gradient, whereby water was increased to 40% over a period of 40 min at a flow rate of 1 ml/min. [U-$^{15}N_5$]-6-OH-PdG and [U-$^{15}N_5$]-8-OH-PdG were prepared in the same manner as their unlabeled counterparts, but on a smaller scale by reacting 100 μg of [U-$^{15}N_5$]-dG with 2 μl of acrolein in 400 μl of 0.025 M phosphate buffer.

[U-$^{15}N_5$]-N^2-ethyl-dG was prepared using a modification of a previous method [25] by reacting 100 μl of AA with a 1 mg/ml solution of [U-$^{15}N_5$]-dG in a total reaction volume of 1 ml at 37 °C in the dark for 12 h. Afterwards, $NaBH_3CN$, approximately 20 mg, was added to the mixture in 30 min intervals over a period of 2 h while the reaction was continued at 37 °C. The resulting solution was subjected to reverse phase column chromatography as described in the clean-up of the acrolein reaction products, vacuum concentrated, redissolved in 200 μl of DMSO and purified also as described above. [U-$^{15}N_5$]-1,N^2-PdG$_1$ and [U-$^{15}N_5$]-1,N^2-PdG$_2$ were prepared by adding 20 μl of crotonaldehyde to 1 ml of [U-$^{15}N_5$]-dG (1 mg/ml) for a reaction time of 12 h at 37 °C and [U-$^{15}N_5$]-εdA was synthesized from [U-$^{15}N_5$]-dA according to a previously published method [26]. Purification of the diastereomers [U-$^{15}N_5$]-1,N^2-PdG$_1$ and [U-$^{15}N_5$]-1,N^2-PdG$_1$, and [U-$^{15}N_5$]-εdA was carried out in the same manner as described in the preparation of [U-$^{15}N_5$]-N^2-ethyl-dG. Unlabeled authentic standards of N^2-ethyl-dG, 1,N^2-PdG$_1$ and 1,N^2-PdG$_2$ were prepared in the same manner as described for each, but with unlabeled deoxyguanosine. Purities of all adduct standards were confirmed by measuring absorbance in a GeneSpec V ultraviolet (UV)–vis spectrophotometer with accompanying software (Hitachi Naka Instruments, Co., Ltd., Tokyo, Japan) and the quantity of each purified standard was measured.

2.3. Esophagus and lung tissue DNA extraction and digestion

Human lung and esophagus tissue were obtained postmortem from a Japanese female aged 78 years and were stored in ethanol at −80 °C until DNA purification. DNA was purified with the Puregene DNA Purification System (Gentra Systems, Minneapolis, MN, USA) according to the manufacturer's instructions and desferroxamine was included in the extraction solutions (final concentration 0.1 mM). DNA was obtained from (1) centrally-located lung tissue, from the region of the right middle lobar bronchus bifurcation, (2) peripherally-located lung tissue, from the distal edge of the right inferior lobe and (3) esophagus tissue, obtained mid-region, approximately equidistant from the pharynx and the cardia. Purified DNA was suspended in 500 μl of distilled water and quantification was carried out by measuring absorbance at 260 and 280 nm in a 50 μl volume quartz cell with a UV–vis spectrophotometer. Based upon DNA concentration, aliquots containing 100 μg of DNA were transferred to 1.5 ml Eppendorf tubes and subjected to vacuum concentration (model CC-105 centrifugal concentrator, Tomy Seiko Co., Tokyo, Japan). Following water removal, lung DNA samples were enzymatically hydrolyzed to their corresponding 2′-deoxyribonucleoside-3′-monophosphates by the addition of 100 μl of MN/SPD buffer (200 mM citrate buffer, 100 mM $CaCl_2$, pH 6.0), plus 10 μl each of MN (15 U/μl) and SPD (0.05 U/μl). Solutions were gently mixed by hand and incubated for 2 h at 37 °C. After incubation, 30 units of alkaline phosphatase, 100 μl of 0.5 M Tris–HCl (pH 8.5), 50 μl of 20 mM $ZnSO_4$ and 700 μl of distilled water were added. The solution was again gently mixed and incubated further for 3 h at 37 °C. After incubation the sample volume was reduced to approximately 40 μl by centrifugal concentration and the tube contents were extracted twice with chilled methanol. To each tube, 300 μl of methanol were added, the tubes were shaken for approximately 3 min at 2500 rpm on an Eyela model CM-100 mixer (Tokyo, Japan) and followed by centrifugation at 15,000 × g at 4 °C for 5 min in a Tomy MTX-150 refrigerated centrifuge (Tomy Seiko Co.). The supernatant extract was removed to a new tube, and the pellet was extracted again with methanol and combined with the previous methanol extract for a total volume of 600 μl. Lastly, the methanol was removed by centrifugal concentration and the remaining 2′-deoxynucleosides were resuspended in 1 ml of a 2 ng/ml solution of ddI internal standard in distilled water. In addition to the esophagus and lung tissue DNA, unreacted calf thymus DNA, 100 μg, was treated in an identical manner prior to LC/ESI-MS/MS analyses.

2.4. Instrumentation

LC/ESI-MS/MS analyses were performed using a Shimadzu HPLC system (Shimadzu) consisting of dual LC-10ADVP pumps and equipped with an SPD-10ADVP UV–vis detector interfaced with a Quattro Ultima triple stage quadrupole mass spectrometer (Micromass, Manchester, UK). The LC column was eluted over a gradient that began at a ratio of 15% methanol to 85% water and was changed to 80% methanol to 20% water over a period of 10 min. The 80:20 conditions were held for 10 min and then returned to the original starting conditions, 15:85, which was held for the remaining 8 min. The total run time was 28 min during which the sample components were delivered to the mass spectrometer by electrospray. Sample injection volumes of 50 μl each were injected by a Shimadzu SIL-10ADVP autoinjector, separated on a Shim-pack FC-ODS, 150 mm × 4.6 mm column (Shimadzu) and eluted at a flow rate of 0.5 ml/min. Mass spectral analyses were carried out in positive ion mode with nitrogen as the nebulizing gas. The ion source temperature was 130 °C, the desolvation temperature was 380 °C, and the cone voltage was operated at a constant 35 V. Nitrogen gas was also used as the desolvation gas (700 l/h) and

cone gas (35 l/h) and argon was used as the collision gas at a collision cell pressure of 1.5×10^{-3} mBar. Positive ions were acquired in MRM mode and the strategy was designed to detect the neutral loss of 2′-deoxyribose from positively ionized 2′-deoxynucleoside adducts by monitoring the samples transmitting their $[M+H]^+ > [M+H-116]^+$ transitions. For each tissue DNA sample, from centrally- and peripherally-located lung tissue and esophagus tissue DNA, 374 MRM transitions were monitored over the *m/z* range from transition *m/z* 228.8 > 112.8 through transition *m/z* 602.8 > 486.8. For each 50 μl sample injection (5 μg of digested DNA on column), a total of 32 channels were monitored simultaneously, with one channel for each injection reserved to monitor the ddI internal standard at transition *m/z* 236.8 > 136.8. By using this strategy, each sample was injected 12 times to complete the monitoring of transitions from *m/z* 228.8 to 602.8.

The unambiguous identification of specific target adducts N^2-ethyl-dG, εdA, 1,N^2-PdG$_1$, 1,N^2-PdG$_2$, 8-OH-PdG and two isomers of 6-OH-PdG was performed by comparison to authentic adduct standards and by stable isotope dilution under the same LC/ESI-MS/MS conditions as explained above except that the flow rate was 0.4 ml/min and the mobile phase was 98% water and 2% methanol, increased linearly to 60% water and 40% methanol for 40 min, further increased to 20% water and 80% methanol for 5 min and then returned to the original starting conditions of 98% water and 2% methanol for a total run time of 60 min. MRM transitions for each adduct type were monitored as follows: [U-$^{15}N_5$]-1,N^2-PdG$_1$, [U-$^{15}N_5$]-1,N^2-PdG$_2$, *m/z* 342.8 > 226.8; 1,N^2-PdG$_1$, 1,N^2-PdG$_2$, *m/z* 337.8 > 221.8; [U-$^{15}N_5$]-6-OH-PdG, [U-$^{15}N_5$]-8-OH-PdG, 329.0 > 213.0; 6-OH-PdG, 8-OH-PdG, 324.0 > 208.0; [U-$^{15}N_5$]-N^2-ethyl-dG, *m/z* 300.9 > 184.9; N^2-ethyl-dG *m/z* 295.9 > 179.9; [U-$^{15}N_5$]-εdA, *m/z* 280.9 > 164.9; εdA, *m/z* 275.9 > 159.9.

2.5. Data processing

Data processing was performed in stages as described previously [24]. First putative DNA adduct peaks were integrated using MassLynx 4.0 Global Mass-Informatics Software, secondly, peak integration data were transferred to a spreadsheet and normalized based upon the quantity of ddI internal standard detected for each injection, thirdly, manual screening for 2′-deoxynucleoside artifacts was carried out as summarized in Table 1. In the final stage of data processing, chromatograms for each $[M+H]^+ > [M+H-116]^+$ transition, from *m/z* 228.8 to 602.8, were analyzed to identify and eliminate DNA adduct "ghost" isotope peaks and data were organized to produce the adductome maps. In the final analysis, bubble-type charts were created whereby the LC column retention time of the putative adduct is indicated on the *x*-axis, the mass to charge ratio of the putative adduct is indicated on the *y*-axis, and the bubble size represents the putative adduct peak integration area normalized by the internal standard peak integration area, and is referred to as the area response.

Table 1
Positively ionized 2′-deoxynucleoside artifacts

Base[a]	$+H^+$	$+NH_4^+$	$+Na^+$	$+K^+$	Dimer + H^+
dC	228.09	245.09	250.09	266.09	455.18
dT	243.09	260.09	265.09	281.09	485.09
dA	252.10	269.10	274.10	290.10	503.20
dG	268.10	285.10	290.10	306.10	535.20
5-Methyl-dC	242.11	259.11	264.11	280.11	483.11

Values are given as *m/z*.
[a] 2′-Deoxycytidine; 2′-deoxythymidine; 2′-deoxyadenosine; 2′-deoxyguanosine.

3. Results and discussion

3.1. Adductome maps of lung, esophagus and calf thymus negative control

Figs. 1 and 2 graphically represent the final analyses for centrally- and peripherally-located lung tissue DNA samples (Fig. 1A and 1B respectively), for esophagus tissue DNA (Fig. 2A) and for negative control calf thymus DNA (Fig. 2B) all organized as adduc-

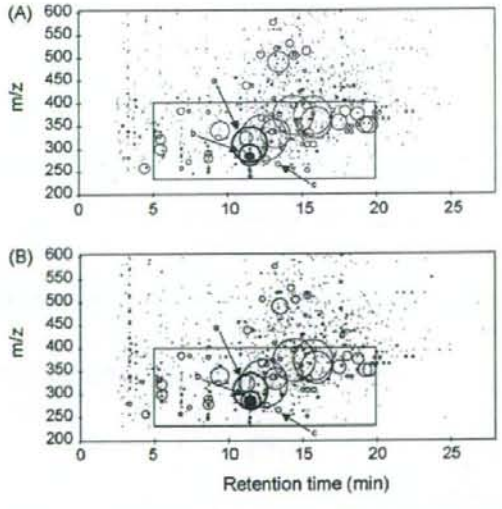

Fig. 1. Two adductome maps of putative DNA adducts detected in central (A) and peripheral (B) human lung tissue DNA from the same individual. The neutral loss of 2′-deoxyribose from positively ionized 2′-deoxynucleoside putative adducts was analyzed by LC/ESI-MS/MS in MRM mode transmitting the $[M+H]^+ > [M+H-116]^+$ transition over a total of 374 transitions in the mass range from *m/z* 228.8 to 602.8. The active zone is indicated by the box and putative adducts *a* through *c* are labeled in the figure and discussed in the text. The blackened bubble (referred to as putative adduct *d* in the text) indicates a putative adduct that was detected at high levels in the DNA of both lung tissue samples but that was detected at a level more than two orders of magnitude lower in esophagus tissue DNA.

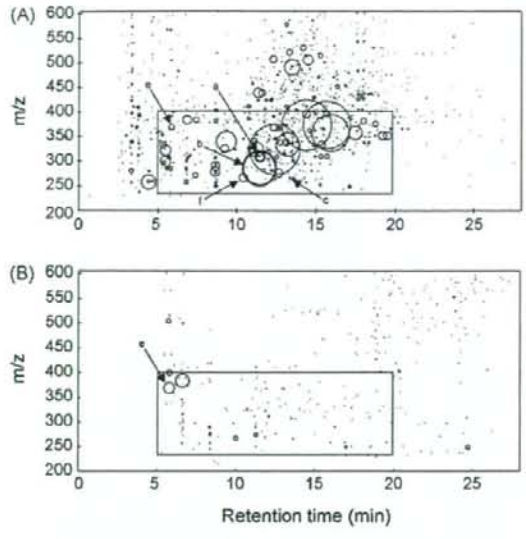

Fig. 2. Adductome maps of putative DNA adducts detected in human esophagus tissue DNA (A) and negative control calf thymus DNA (B). The active zone is indicated by the box and putative adducts *a* through *f* are labeled in the figure and discussed in the text.

tome maps. Putative DNA adducts were more or less detected over the entire *m/z* range in all cases and based upon the observed putative adduct bubble sizes and pattern formations in each adductome map, a high degree of similarity among the two lung tissue DNA samples and the esophagus tissue DNA sample was revealed (Fig. 1A and B and Fig. 2A). These results are in strong contrast to the adductome map of a negative control produced as a result of DNA digestion, LC/ESI-MS/MS analysis and data processing of calf thymus DNA (Fig. 2B).

In lung and esophagus tissue DNA samples, adductome mapping revealed that the most abundant putative adducts occurred similarly in many cases and with similar area response values, but clear differences were also revealed. In all three samples, the highest zone of activity was detected between 5 and 20 min for putative adducts that possessed *m/z* values approximately less than 400 and this zone is indicated in Figs. 1 and 2 by the rectangular box. This active zone, defined by large numbers of putative adducts that possessed the highest area response values, is similar to that which was shown to occur previously in lung tissue DNA taken from a smoker and non-smoker [24]. However, when these data are compared to previous adductome analyses of lung tissue DNA, the most abundant putative adducts detected in this study were markedly different compared to the most abundant putative adducts detected prior, and in addition, these new putative adducts possessed area response values that were up to two orders of magnitude greater than the most abundant putative adducts detected before. Considering these limited data sets, for now it may simply be concluded that such differences reflect the exposure profiles and metabolism of the individuals from whom the DNA was obtained. Of particular interest in regard to the above situation was that the seven most abundant putative adducts detected in lung in the previous study [24] were also detected in the two lung adductome analyses performed in this study. Additionally, a comparison of the average area response values of the putative adducts from these two separate studies indicated that the average area response values did not differ by any order of magnitude, but were in fact found to be quite similar as shown in Table 2. For this analysis, the most abundant putative adducts in the previous study were defined whereby at least one putative adduct of a putative adduct pair possessed an area response value greater than 10; seven putative adducts qualified. Indeed, as indicated in Table 2, after matching putative adducts from the two different studies by retention time and *m/z*, the similarities between the average area response values of previously analyzed lung tissue DNA samples and lung tissue DNA samples from this study ranged from almost equal to approximately only six times different (in one case, *m/z* 323.8) and no differences occurred by an order of magnitude. These data indicate that these putative adducts may be relatively conserved at these levels in lung tissue and may lend support to data set validation by indicating that the most abundant putative adducts detected in this study were a result of a more specific exposure or circumstances. Of course, further adductome analyses of lung tissue DNA samples are necessary and as such analyses are performed, a clearer pattern may emerge.

3.2. Comparison of putative adducts

From all three tissue DNA samples, the 50 most abundant adducts, based upon area response, were aligned by *m/z* and retention time and compared ($n = 50$). The two lung samples shared 90% similarity, while esophagus DNA was 84 and 80% similar to peripheral lung DNA and central lung DNA respectively. The area response values of the most abundant 50 putative adducts represented approximately 85% of the total area response values of all putative adducts detected in each of the three samples ($85.6 \pm 0.4\%$, $n = 3$) while the largest 20, 30 and 100 putative adducts represented approximately the 76th, 81st and 90th percentiles respectively with little standard deviation among the three samples: 76.8 ± 0.8,

Table 2
Similarity of the average area response values of the most abundant putative adducts in lung tissue DNA from a previous study ($n=7$) and the corresponding identical putative adducts observed in lung tissue DNA in this study

m/z	Lung tissue DNA from previous study[a]		Lung tissue DNA from this study	
	R/T (min)[b]	Area response[c]	*R/T* (min)	Area response
257.8	4.43–4.47	24.9 ± 0.5	4.41–4.43	28.7 ± 7.3
278.8	8.68–8.72	17.6 ± 4.3	8.66–8.73	31.0 ± 5.2
283.8	11.46–11.50	51.1 ± 15.9	11.44–11.48	25.6 ± 1.6
289.8	8.68–8.70	17.2 ± 2.8	8.64–8.73	20.7 ± 3.4
323.8	11.25–11.27	12.2 ± 4.9	11.19–11.23	74.2 ± 13.0
337.8	13.08–13.12	12.1 ± 7.9	13.10	13.7 ± 0.7
383.8	6.89–6.91	25.5 ± 3.0	6.81–6.87	18.9 ± 0.2

[a] Kanaly et al. [24].
[b] LC retention time, based upon putative adduct peak height maxima and indicated as a range. In one instance where the putative adduct peak maxima were identical, no range is indicated.
[c] Average area response values of lung DNA putative adduct pairs with the range indicated. The area response value is equal to the putative DNA adduct LC chromatogram peak integration area normalized by the internal standard LC chromatogram peak integration area, ddI.

81.3 ± 0.7 and 90.0 ± 0.3% respectively, $n=3$ in each case. Considering that over 1000 putative adducts were detected in each of the three tissue samples, and that the most abundant 20–100 putative adducts represented 76–90% of the total number of adducts by area response value, it seems prudent to focus our investigative attention on these putative adducts which occur in the most abundant 20–100 putative adducts at this time in the early development of the technique. Study continuation with multiple samples from the same tissues of the same individual and coupled with comparisons to other individuals shall increase our understanding in regard to the range of intratissue, intertissue and interindividual DNA adduct variation.

3.3. Intertissue variation revealed by the final analyses

By organizing the final analyses as adductome maps, similarities and some differences were revealed between the three tissue samples. In Fig. 1, attention is drawn to the presence of four putative adducts that were detected with relatively similar area response values in the active zone of the two lung DNA samples. These four unidentified putative adducts are designated in the adductome maps by letters *a* through *c* with a fourth putative adduct bubble blackened for the purpose of reducing any confusion in regard to the putative adduct designations and is hereafter referred to as putative adduct *d*. As mentioned, these four putative adducts: (*a*) *m/z* 307.8, *R/T* 11.46–11.48 (where *R/T* is retention time); (*b*) *m/z* 285.8, *R/T* 11.48; (*c*) *m/z* 265.8, *R/T* 13.36–13.40 and (*d*) *m/z* 283.8, *R/T* 11.44–11.48 all possessed relatively similar area response values in lung tissue but were found to be different when compared to esophagus tissue (Fig. 2A). Although the reasons for these differences are not clear now, such differences may represent differential DNA adduct susceptibility between the lungs and esophagus. For example, putative adduct *a* was detected at nearly equal high levels in both lung tissue DNA samples (area response = 388.4 ± 13.8; difference = ±3.6%) but was more than an order of magnitude lower in esophagus DNA (area response = 27.3; approximately 14 times lower). As shown in Figs. 1 and 2 Figs. 1A, 1B and 2A, although putative adduct *b* was detected at relatively high levels in all three samples – the average area response value was equal to 131.0 ± 17.8 in lung tissue DNA – it was detected at more than twice that level in esophagus tissue DNA (area response = 296.0). Adductome mapping also revealed that putative adducts *c* and *d* occurred to larger extents and at relatively equal levels in lung tissue DNA but occurred to a lesser extent (putative adduct *c*) or did not appear at all in the adductome map of esophagus tissue DNA (putative adduct *d*). The utility of representing the final analyses as adductome maps for comparing intertissue variation is adequately illustrated in the case of putative adduct *d*. Map comparisons (Figs. 1 and 2) clearly indicate the similarities and differences among the four DNA samples. After attention was drawn to putative adduct *d*, it was later determined that it was indeed detected in esophagus tissue DNA but to an extent that was too small to appear in maps of this scale. The area response value of putative adduct *d* in esophagus tissue DNA was 0.14, a level that was more than two orders of magnitude lower than that detected in lung tissue DNA.

Additionally, adductome mapping revealed at least two cases whereby putative adducts were detected at rel-

atively high levels in esophagus tissue DNA (Fig. 2A) but not in lung tissue DNA (Fig. 1A and B). As shown in Fig. 2A, putative adducts *e* and *f* were detected in esophagus tissue DNA (area response values = 11.3 and 21.8 respectively) but were detected at greater than 7- and 10-fold lower levels in lung tissue DNA (average area response values = 1.6 ± 0.1 and 1.9 ± 0.1 respectively) and did not appear in the adductome maps from lung tissue DNA. As shown in the adductome map in Fig. 2B, putative adduct *e* was detected at the highest level overall in calf thymus DNA, area response equal to 35.1, which was three times higher than the level detected in esophagus tissue DNA. Clearly indicated in Fig. 2B was that application of the adductome mapping technique to calf thymus DNA revealed low numbers of adducts that possessed high area response values. Although these data lend support to the validity of the technique, more sample analyses are required, including the assessment of other DNA samples that may serve as appropriate negative controls. For example, salmon testes, human placenta and bacterial DNA have been useful for this purpose in the past [16].

3.4. Unambiguous adduct identification in tissue samples and assignment of adduct identities in adductome maps

Fig. 3 shows identical areas of an expansion of the active zone of the adductome maps created for central lung tissue DNA and esophagus tissue DNA in Figs. 1A and 2A respectively. The retention time ranges from 5 to 20 min and the mass to charge ratio ranges from *m/z* 250 to 375 in these expansion charts. Indeed, included in this *m/z* range and retention time range are all putative adducts previously discussed in Figs. 1 and 2 and they are indicated in Fig. 3 for reference. Noteworthy are that the presence of putative adducts *e* and *f* were revealed in lung tissue DNA by this expansion, but that the level of putative adduct *d* was still too low to be detected. Indeed, the area response value of putative adduct *d* differed by more than order of magnitude from putative adducts *e* and *f*.

A major issue for expanding the power of the final analyses and validating the adductome mapping technique is the unambiguous assignment of identities to the putative adducts that appear in the maps. This process is paramount to the usefulness of the technique in the future. Considering this, four DNA adduct standards, 1,N^2-PdG$_1$, 1,N^2-PdG$_2$, N^2-ethyl-dG and εdA, and their [U-^{15}N$_5$]-stable isotope analogues were synthesized and used to assay for the presence of these adducts in lung tissue and esophagus tissue DNA by LC/ESI-MS/MS.

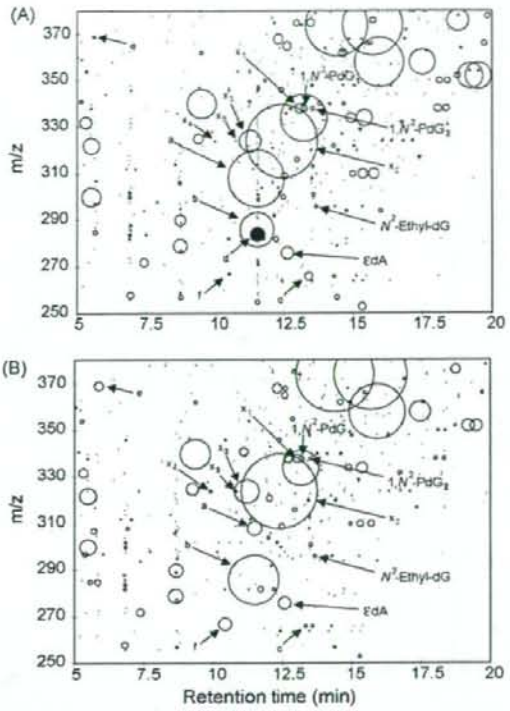

Fig. 3. Expansion of identical areas of the active zone from central lung tissue DNA (A) and esophagus tissue DNA (B) taken from the adductome maps in Figs. 1A and 2A. The exact positions of four DNA adducts whose identities were initially confirmed: 1,N^2-PdG$_1$, 1,N^2-PdG$_2$, N^2-ethyl-dG and εdA are indicated directly in the figure. They were identified by comparison to authentic standards and by radioisotope dilution LC-ESI/MS/MS. Putative adducts x_1 through x_5 and putative adducts *a* through *f* are indicated in the figure and discussed in detail in the text.

These adducts were unambiguously detected in all three tissue DNA samples and their exact positions in the adductome maps were determined as indicated in Fig. 3. Identification of each adduct was made by comparison to authentic standards using an identical LC elution gradient as used for adductome map analyses (as shown for 1,N^2-PdG$_1$ and 1,N^2-PdG$_2$ in lung tissue DNA in Fig. 4A and B for example) and in conjunction with unambiguous identification by spiking of [U-^{15}N$_5$]-stable isotope standards into lung tissue and esophagus tissue samples post-digestion followed by LC/ESI-MS/MS re-analysis utilizing higher resolution LC conditions (as shown for εdA in lung tissue DNA in Fig. 4C and D for example). Based upon our understanding that the most abundant 100 putative adducts detected in this study represented 90% of the number of putative adducts by area response

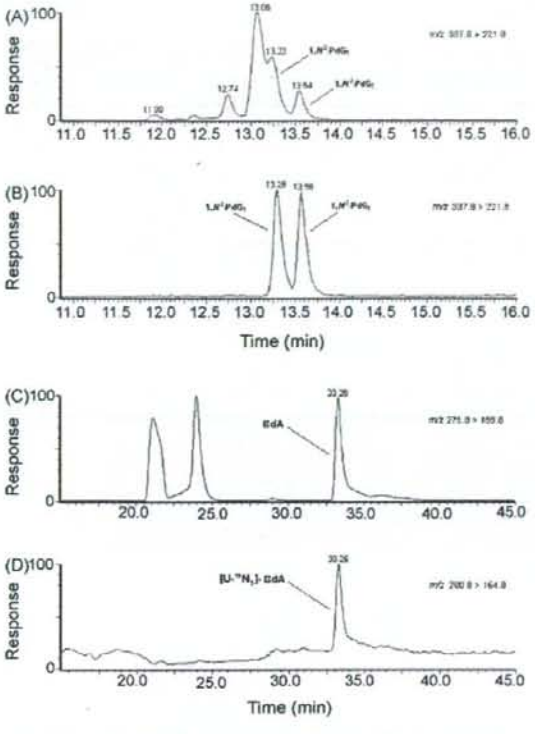

Fig. 4. LC/ESI-MS/MS detection of adducts in DNA obtained from centrally-located human lung tissue by comparison to authentic standards and by stable isotope dilution. (A) Lung tissue sample DNA compared to (B) 1,N^2-PdG$_1$ and 1,N^2-PdG$_2$ authentic standards (m/z 337.8 > 221.8); (C) lung tissue DNA (m/z 275.8 > 159.8) compared to (D) [U-$^{15}N_5$]-εdA (m/z 280.8 > 164.8). The LC retention times are indicated above the peaks in minutes.

in these samples, it was notable that three of the four positively identified adducts fell into this range. εdA was detected with relatively high area response values overall and represented the 20th most abundant adduct detected in esophagus tissue for example. N^2-ethyl-dG was the exception and did not occur within the most abundant 100 putative adducts for any sample, but was detected within the most abundant 150 putative adducts in all three cases. Identification of adduct map positions contributes to our overall view of the adductome maps and represents the beginning of the process of attaching identities to putative adducts revealed by the adductome mapping technique. Clearly, the adductome maps revealed the presence of many unidentified abundant putative adducts over a wide molecular weight range and it shall be a challenge to either attach identities to these putative adducts or re-adjust the final analyses based upon the results of future research.

3.5. Refining the process of adductome map creation

In addition to putative adducts *a* through *f* and the unambiguously identified adducts discussed above, five further putative adduct designations (x_1 through x_5) are indicated in the adductome maps in Fig. 3. Putative adduct x_1 (m/z 337.8) was revealed in a previous study to be one of the most abundant putative adducts in the lung tissue DNA of a smoker [24]. Based upon its mass to charge ratio it was hypothesized that it might be 1,N^2-PdG$_1$ or 1,N^2-PdG$_2$. Synthesis of stable isotopes of 1,N^2-PdG$_1$ and 1,N^2-PdG$_2$ followed by stable isotope dilution analyses showed that this was not to be the case although 1,N^2-PdG$_1$ and 1,N^2-PdG$_2$ were identified in the sample. When putative adduct x_1 was analyzed under higher resolution LC conditions, five smaller peaks were further resolved to elute with x_1 and based upon the literature it was discussed that these peaks may have represented isomers of the DNA adducts of 1,N^2-propano-dG [24]. In this study, this putative adduct was detected again in lung and esophagus tissues samples except that the area response values for each putative adduct x_1 were all more than half of the value encountered for the smoker in the previous study.

The most abundant putative adduct in both lung tissue samples as indicated in the adductome maps in Figs. 1–3 was putative adduct x_2 which possessed an m/z value of 323.8, retention time range of 12.39–12.41 and an area response value equal to 681.8 ± 11.9. In esophagus tissue DNA, putative adduct x_2 occurred similarly and was the second most abundant putative adduct; retention time = 12.39, area response = 686.7. Due to its large area response value, the identity of this putative adduct was checked by synthesizing and purifying three DNA adduct standards of acrolein (8-OH-PdG and two isomers of 6-OH-PdG) which all possess molecular weights of approximately 323. Acrolein was reacted with dG and the ^{15}N-stable isotope analogue of dG as explained in the Section 2, HPLC profiles similar to that shown to occur in previous studies were observed [27,28] and reaction products were purified as 8-OH-PdG and the two stereosiomers of 6-OH-PdG. Utilization of these acrolein-derived DNA adduct standards in further LC/ESI-MS/MS analyses allowed for the identification of these adducts in all three tissue samples and their locations were identified on the adductome maps in Fig. 3A and B; large putative adduct x_3 was identified as 8-OH-PdG and putative adducts x_4 and x_5 were identified as stereoisomers of 6-OH-PdG. Although these analyses confirmed the presence of acrolein-derived adducts in the three samples, the identity of putative adduct x_2

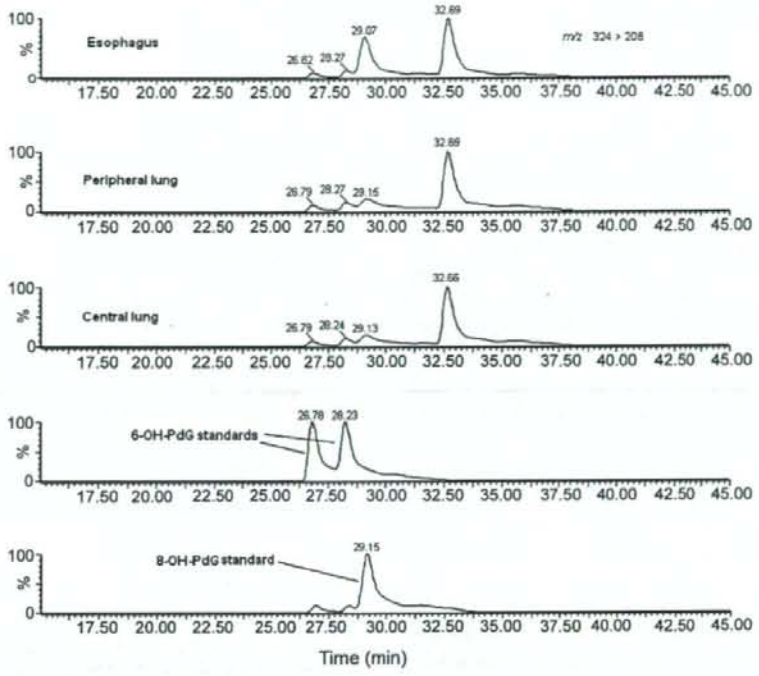

Fig. 5. 6-OH-PdG and 8-OH-PdG adduct detection by LC/ESI-MS/MS in human lung and esophagus tissue DNA by comparison to authentic standards of 6-OH-PdG and 8-OH-PdG (*m/z* 324 > 208). The LC retention times are indicated above the peaks in minutes.

remained unknown. Fig. 5 shows the confirmation of 6-OH-PdG and 8-OH-PdG in all lung and esophagus tissue DNA samples by comparison to authentic 6-OH-PdG and 8-OH-PdG standards.

Overall, a total of seven DNA adducts, N^2-ethyl-dG plus six potentially endogenously- and/or exogenously-produced oxidative adducts, 1,N^2-PdG$_1$, 1,N^2-PdG$_2$, εdA, 8-OH-PdG, and two isomers of 6-OH-PdG were unambiguously detected in all tissue DNA samples in this study and their positions in the adductome maps were located. Indeed, all of these adducts have been detected in humans in different studies and at various levels before [22,29–31]. Exposure to bifunctional electrophilic enals (α,β-unsaturated aldehydes) such as acrolein and crotonaldehyde, through cigarette smoke for example, or through endogenous metabolism via lipid peroxidation may result in the propano adducts identified in this study. Through DNA exposure to exogenous chemicals like urethane, or if enals are converted to more DNA-reactive epoxyaldehydes through cellular oxidative processes, etheno adducts such as εdA may result [1]. Additionally, exposure to acetaldehyde from the environment or through alcohol or tobacco consumption may result in the formation of N^2-ethyl-dG adducts [32].

3.6. Conclusions

Application of the adductome approach for the assessment of intertissue DNA adduct variation was presented for the first time. Assessment of human lung and esophagus tissue DNA revealed many similarities and some distinct differences in the types and abundances of putative adducts detected in the three tissue DNA samples. This assessment demonstrated the utility of the adductome mapping technique by facilitating the visualization of putative adduct detection patterns and their relative levels of occurrence. Application of the adductome approach to calf thymus DNA as a negative control revealed that few putative adducts occurred with high area response values and provided further validation of the technique when compared to tissue DNA samples.

Through the mapping technique, clear similarities and clear differences between the tissue samples were revealed and these allowed for further exploration of those putative adducts of interest. Putative adducts in lung tissue DNA were shown to be 90% similar by this technique while putative adducts in esophagus tissue DNA were shown to be only 80 and 84% similar to central and peripheral lung tissue DNA respectively.

Although over 1000 putative adducts were detected in each of the three tissue DNA samples, analysis indicated that the largest-occurring 100 putative adducts represented 90% of all putative adducts detected in each sample. Unambiguous identification of seven DNA adducts by comparison to authentic adduct standards and stable isotope dilution was performed for all three samples and DNA adduct identities were attached to putative adducts detected by the adductome mapping technique. In terms of technique feasibility, further refinement shall be required such that (1) LC peak resolution is confirmed as adequate, (2) the time required per sample injection is reasonable for the processing of high numbers of samples, (3) data analyses can be completed in a manageable period of time and (4) further validation of reproducibility in terms of adduct type detection and adduct abundance are resolved. Indeed, the attainment of a more appropriate balance of these variables represents one of the challenges in refining the adductome approach for analyzing large numbers of samples.

In closing, the creation of adductome maps from different tissue DNA samples facilitated the visualization of putative DNA adducts and allowed for comprehensive comparisons between samples that would otherwise prove to be difficult. As we continue to assign identities to the putative adducts that are revealed by this methodology, tissue-specific or exposure-specific patterns may continue to emerge and provide further insight on DNA adduct formation in humans.

Acknowledgements

This work was supported in part by grants-in-aid for cancer research from the Japanese Ministry of Health, Labor and Welfare, for scientific research (15681002) from MEXT, Japan, from NEDO, Japan and by the Japan Society for the Promotion of Science (JSPS). We thank Dr. Kentaro Misaki, Kyoto University for synthesizing [U-$^{15}N_5$]-εdA.

References

[1] R. De Bont, N. van Larebeke, Endogenous DNA damage in humans: a review of quantitative data, Mutagenesis 19 (2004) 169–185.

[2] G.N. Wogan, S.S. Hecht, J.S. Felton, A.H. Conney, L.A. Loeb, Environmental and chemical carcinogenesis, Semin. Cancer Biol. 14 (2004) 473–486.

[3] S. Bjelland, E. Seeberg, Mutagenicity, toxicity and repair of DNA base damage induced by oxidation, Mutat. Res. 531 (2003) 37–80.

[4] M.S. Cooke, M.D. Evans, M. Dizdaroglu, J. Lunec, Oxidative DNA damage: mechanisms, mutation, and disease, FASEB J. 17 (2003) 1195–1214.

[5] M.S. Cooke, R. Olinski, M.D. Evans, Does measurement of oxidative damage to DNA have clinical significance? Clin. Chim. Acta 365 (2005) 30–49.

[6] L.J. Marnett, J.N. Riggins, J.D. West, Endogenous generation of reactive oxidants and electrophiles and their reactions with DNA and protein, J. Clin. Invest. 111 (2003) 583–593.

[7] W.L. Neeley, J.M. Essigmann, Mechanisms of formation, genotoxicity, and mutation of guanine oxidation products, Chem. Res. Toxicol. 19 (2006) 491–505.

[8] G. Slupphaug, B. Kavli, H.E. Krokan, The interacting pathways for prevention and repair of oxidative DNA damage, Mutat. Res. 531 (2003) 231–251.

[9] D.H. Phillips, DNA adducts as markers of exposure and risk, Mutat. Res. 577 (2005) 284–292.

[10] R.M. Santella, M. Gammon, M. Terry, R. Senie, J. Shen, D. Kennedy, M. Agrawal, B. Faraglia, F.-F. Zhang, Mutat. Res. 592 (2005) 29–35.

[11] A. Rundle, Carcinogen-DNA adducts as a biomarker for cancer risk, Mutat. Res. 600 (2006) 23–36.

[12] P.B. Farmer, K. Brown, E. Tompkins, V.L. Emms, D.J.L. Jones, R. Singh, D.H. Phillips, DNA adducts: mass spectrometry methods and future prospects, Toxicol. Appl. Pharmacol. 207 (2005) 293–301.

[13] H. Koc, J.A. Swenberg, Applications of mass spectrometry for quantitation of DNA adducts, J. Chromatogr. B 778 (2002) 323–343.

[14] R. Singh, P.B. Farmer, Liquid chromatography-electrospray ionization-mass spectrometry: the future of DNA adduct detection, Carcinogenesis 27 (2006) 178–196.

[15] F.A. Beland, M.I. Churchwell, L.S. Von Tungeln, S. Chen, P.P. Fu, S.J. Culp, B. Schoket, E. Gyorffy, J. Minárovits, M.C. Poirier, E.D. Bowman, A. Weston, D.R. Doerge, High-performance liquid chromatography electrospray ionization tandem mass spectrometry for the detection and quantitation of benzo[a]pyrene-DNA adducts, Chem. Res. Toxicol. 18 (2005) 1306–1315.

[16] D.R. Doerge, M.I. Churchwell, J.-L. Fang, F.A. Beland, Quantification of etheno-DNA adducts using liquid chromatography, on-line sample processing, and electrospray tandem mass spectrometry, Chem. Res. Toxicol. 13 (2000) 1259–1264.

[17] X. Liu, M.A. Lovell, B.C. Lynn, Detection and quantification of endogenous cyclic DNA adducts derived from trans-4-hydroxy-2-nonenal in human brain tissue by isotope dilution capillary liquid chromatography nanoelectrospray tandem mass spectrometry, Chem. Res. Toxicol. 19 (2006) 710–718.

[18] E.M. Ricicki, J.R. Soglia, C. Teitel, R. Kane, F. Kadlubar, P. Vouros, Detection and quantification of *N*-(deoxyguanosin-8-yl)-4-aminobiphenyl adducts in human pancreas tissue using capillary liquid chromatography-microelectrospray mass spectrometry, Chem. Res. Toxicol. 18 (2005) 692–699.

[19] N.M. Thomson, R.S. Mijal, R. Ziegel, N.L. Fleischer, A.E. Pegg, N.Y. Tretyakova, L.A. Peterson, Development of a quantitative liquid chromatrography/electrospray mass spectrometric assay for a mutagenic tobacco specific nitrosamine-derived DNA adduct, O^6-[4-oxo-4-(3-pyridyl)butyl]-2′-deoxyguanosine, Chem. Res. Toxicol. 17 (2004) 1600–1606.

[20] M.I. Churchwell, F.A. Beland, D.A. Doerge, Quantification of multiple DNA adducts formed through oxidative stress using liquid chromatography and electrospray tandem mass spectrometry, Chem. Res. Toxicol. 15 (2002) 1295–1301.

[21] A. Barbin, H. Ohgaki, J. Nakamura, M. Kurrer, P. Kleihues, J.A. Swenberg, Endogenous deoxyribonucleic acid (DNA) damage in human tissues: a comparison of ethenobases with aldehydic

DNA lesions. Cancer Epidemiol, Biomarkers Prev. 12 (2003) 1241–1247.

[22] R. Godschalk, J. Nair, F.J. van Schooten, A. Risch, P. Drings, K. Kayser, H. Dienemann, H. Bartsch, Comparison of multiple DNA adduct types in tumor adjacent human lung tissue: effect of cigarette smoking, Carcinogenesis 23 (2002) 2081–2086.

[23] F.F. Kadlubar, K.E. Anderson, S. Häussermann, N.P. Lang, G.W. Barone, P.A. Thompson, S.L. MacLeod, M.W. Chou, M. Mikhailova, J. Plastaras, L.J. Marnett, J. Nair, I. Velic, H. Bartsch, Comparison of DNA adduct levels associated with oxidative stress in human pancreas, Mutat. Res. 405 (1998) 125–133.

[24] R.A. Kanaly, T. Hanaoka, H. Sugimura, H. Toda, S. Matsui, T. Matsuda, Development of the adductome approach to detect DNA damage in humans, Antoxid. Redox Signal. 8 (2006) 993–1001.

[25] M. Sako, H. Kawada, K. Hirota, A convenient method for the preparation of N^2-ethylguanine nucleosides and nucleotides, J. Org. Chem. 64 (1999) 5719–5721.

[26] P. Raboisson, A. Baurand, J.-P. Cazenave, C. Gachet, M. Retat, B. Spiess, J.-J. Bourguignon, Novel antagonists acting at the P2Y1 purigenic receptor: synthesis and conformational analysis using potentiometric and nuclear magnetic resonance titration techniques, J. Med. Chem. 45 (2002) 962–972.

[27] G. Cheng, Y. Shi, S.J. Sturla, J.R. Jalas, E.J. McIntee, P.W. Villalta, M. Wang, S.S. Hecht, Reactions of formaldehyde plus acetaldehyde with deoxyguanosine and DNA: formation of cyclic deoxyguanosine adducts and formaldehyde cross-links, Chem. Res. Toxicol. 16 (2003) 145–152.

[28] X. Liu, M.A. Lovell, B.C. Lynn, Development of a method for quantification of acrolein-deoxyguanosine adducts in DNA using isotope dilution-capillary LC/MS/MS and its application to human brain tissue, Anal. Chem. 77 (2005) 5982–5989.

[29] J.-L. Fang, C.E. Vaca, Detection of DNA adducts of acetaldehyde in peripheral white blood cells of alcohol abusers, Carcinogenesis 18 (1997) 627–632.

[30] R.G. Nath, F.-L. Chung, Detection of exocyclic 1,N^2-propanodeoxyguanosine adducts as common DNA lesions in rodents and humans, Proc. Natl. Acad. Sci. USA 91 (1994) 7491–7495.

[31] R.G. Nath, J.E. Ocando, J.B. Guttenplan, F.-L. Chung, 1,N^2-Propanodeoxyguanosine adducts: potential new biomarkers of smoking-induced DNA damage in human oral tissue, Cancer Res. 58 (1998) 581–584.

[32] D. Pluskota-Karwatka, A.J. Pawowicz, L. Kronberg, Formation of malonaldehyde-acetaldehyde conjugate adducts in calf thymus DNA, Chem. Res. Toxicol. 19 (2006) 921–926.

Carcinogenesis vol.28 no.11 pp.2363–2366, 2007
doi:10.1093/carcin/bgm057
Advance Access publication March 14, 2007

Increased formation of hepatic N^2-ethylidene-2′-deoxyguanosine DNA adducts in *aldehyde dehydrogenase 2*-knockout mice treated with ethanol

Tomonari Matsuda*, Akiko Matsumoto[1], Mitsuhiro Uchida, Robert A. Kanaly[2], Kentaro Misaki, Shinya Shibutani[3], Toshihiro Kawamoto[4], Kyoko Kitagawa[5], Keiichi I.Nakayama[6], Katsumaro Tomokuni[1] and Masayoshi Ichiba[1]

Graduate School of Global Environmental Studies, Kyoto University, Kyoto 606-8501, Japan, [1]Department of Social and Environmental Medicine, Saga Medical School, Saga 849-8501, Japan, [2]Department of Environmental Biosciences, Yokohama City University, Yokohama, Kanagawa 236-0027, Japan, [3]Department of Pharmacological Sciences, State University of New York at Stony Brook, Stony Brook, NY 11794-8651, USA, [4]Department of Environmental Health, University of Occupational and Environmental Health, Kitakyusyu, Fukuoka 807-8555, Japan, [5]First Department of Biochemistry, Hamamatsu University School of Medicine, Hamamatsu, Shizuoka 431-3192, Japan and [6]Department of Molecular and Cellular Biology, Medical Institute of Bioregulation, Kyusyu University, Fukuoka 812-8582, Japan

*To whom correspondence should be addressed. Tel: +75 753 5052
Fax: +81 75 753 3335;
Email: matsuda@eden.env.kyoto-u.ac.jp
Correspondence may also be addressed to Masayoshi Ichiba.
Fax: +81 952 34 2065;
Email: ichiba@cc.saga-u.ac.jp

N^2-ethylidene-2′-deoxyguanosine (N^2-ethylidene-dG) is a major DNA adduct induced by acetaldehyde. Although it is unstable in the nucleoside form, it is relatively stable when present in DNA. In this study, we analyzed three acetaldehyde-derived DNA adducts, N^2-ethylidene-dG, N^2-ethyl-2′-deoxyguanosine (N^2-Et-dG) and α-methyl-γ-hydroxy-1,N^2-propano-2′-deoxyguanosine (α-Me-γ-OH-PdG) in the liver DNA of *aldehyde dehydrogenase* (*Aldh*)-2-knockout mice to determine the influence of alcohol consumption and the *Aldh2* genotype on the levels of DNA damage. In control *Aldh2*+/+ mice, the level of N^2-ethylidene-dG adduct in liver DNA was 1.9 ± 0.7 adducts per 10^7 bases and was not significantly different than that of *Aldh2*+/− and −/− mice. In alcohol-fed mice (20% ethanol for 5 weeks), the adduct levels of *Aldh2*+/+, +/− and −/− mice were 7.9 ± 1.8, 23.3 ± 4.0 and 79.9 ± 14.2 adducts per 10^7 bases, respectively, and indicated that adduct level was alcohol and Aldh2 genotype dependent. In contrast, an alcohol- or *Aldh2* genotype-dependent increase was not observed for α-Me-γ-OH-PdG, and N^2-Et-dG was not detected in any of the analyzed samples. In conclusion, the risk of formation of N^2-ethylidene-dG in model animal liver *in vivo* is significantly higher in the *Aldh2*-deficient population and these results may contribute to our understanding of *in vivo* adduct formation in humans.

Introduction

Alcohol consumption is a risk factor for hepatocellular carcinoma and acetaldehyde, a carcinogenic intermediate of ethanol, has been suggested to be involved in the occurrence of hepatocellular carcinoma. Two large-scale epidemiological studies revealed that habitual alcohol drinking was probably lead to an increased risk of hepatocellular carcinoma and that a lack of acetaldehyde-metabolizing enzyme activity [aldehyde dehydrogenase (ALDH)-2] was associated with this increased risk (1,2).

There are several enzymes responsible for metabolizing alcohol in the liver. The first step is oxidization of ethanol to acetaldehyde by alcohol dehydrogenase (ADH) and the ADH holoenzyme may exist as either a homodimer or heterodimer of α, β and γ subunits, encoded by *ADH1*, *ADH2* and *ADH3*, respectively. The second step is oxidation of acetaldehyde to acetic acid by ALDH or inducible cytochrome P450 2E1. Human ALDH isozymes are divided into two groups determined by their Michaelis constant values for acetaldehyde: the low K_m ALDH (ALDH1 and ALDH2) and high K_m ALDH (ALDH3 and ALDH4). The K_m values of ALDH3 and ALDH4 are on the order of millimolar (5–83 mM) (3), cytosolic ALDH1 is on the order of micromolar (180 μM) and mitochondrial ALDH2 is on the order of nanomolar (200 nM) (4), suggesting that ALDH2 is a key enzyme responsible for catalyzing oxidation acetaldehyde in human liver. Approximately 40% of Japanese have a mutation in the *ALDH2* gene whereas most Caucasians and Africans do not (5). ALDH2 is a homotetrameric enzyme and the mutant *ALDH2*2* allele (Glu487Lys) encodes for a catalytically inactive subunit (6). It is predicted that individuals who possess the *ALDH2*1/2*2* genotype will have only 6.25% of the normal ALDH2 protein and that other tetramers containing one or more of the ALDH2*2 subunits are mostly inactive. However, when taken together, the overall measured activity of the five possible tetramer combinations of the *ALDH2*1/2*2* genotype is ~13% (7,8). Lastly, individuals who are *ALDH2*2/2*2* homozygous have little ALDH2 activity.

Acetaldehyde itself is a carcinogen that induced nasal tumors in experimental animals by inhalation (9), and is thought to be a tumor initiator because of its mutagenic and DNA-damaging properties (10–13). Recently, we developed an analytical method for acetaldehyde-derived stable DNA adducts, N^2-ethyl-2′-deoxyguanosine (N^2-Et-dG), α-*S*- and α-*R*-methyl-γ-hydroxy-1,N^2-propano-2′-deoxyguanosine (α-*S*-Me-γ-OH-PdG and α-*R*-Me-γ-OH-PdG) by using sensitive liquid chromatography tandem mass spectrometry (LC/MS/MS) (14). Other than these stable DNA adducts, the reaction of acetaldehyde with deoxyguanosine results in the formation of an unstable Schiff base at the N^2 position of deoxyguanosine [N^2-ethylidene-2′-deoxyguanosine (N^2-ethylidene-dG)] (Figure 1). Wang *et al.* (15) showed that N^2-ethylidene-dG in human liver DNA is relatively stable and that the presence of this adduct could be confirmed by detection of N^2-Et-dG after reduction of DNA during isolation and enzymatic hydrolysis. They showed that when the reduction step was included during these steps that approximately a few 100 times more N^2-Et-dG was detected in some cases. In this study, we analyzed these acetaldehyde-derived DNA adducts in the liver DNA of *Aldh2*-knockout mice that were exposed to alcohol to determine the effects of alcohol consumption and the *Aldh2* genotype on the levels of DNA damage in the target organ.

Abbreviations: ADH, alcohol dehydrogenase; ALDH, aldehyde dehydrogenase; εdA, 1,N^6-etheno-2′-deoxyadenosine; LC/MS/MS, liquid chromatography tandem mass spectrometry; α-Me-γ-OH-PdG, α-methyl-γ-hydroxy-1,N^2-propano-2′-deoxyguanosine; N^2-Et-dG, N^2-ethyl-2′-deoxyguanosine; N^2-ethylidene-dG, N^2-ethylidene-2′-deoxyguanosine.

Materials and methods

Aldh2-knockout mice

Aldh2-knockout mice, which had been backcrossed with C57BL6, were obtained from the Department of Environmental Health, University of Occupational and Environmental Health, Japan. Male mice, aged 10–11 weeks old, were used in conformity with the regulations of the committee on animal experiments of Saga University, Japan. The genomic DNA of all subjects was extracted twice—from a small part of the ear and the lung—and the genotype of Aldh2 was determined by polymerase chain reaction according to the method of Kitagawa *et al.* (16).

Alcohol feeding

Male mice were fed an ethanol solution (20%) and standard hard feed CR-LPF (348 kcal/100 g) (Charles River Japan, Yokohama, Japan) for 5 weeks. The number of mice ranged from four to six per group. After 5 weeks, the mice were killed and liver tissue specimens were removed immediately after blood collection, and then parts of the tissue specimens were frozen in liquid nitrogen and stored at −80°C until they were analyzed.

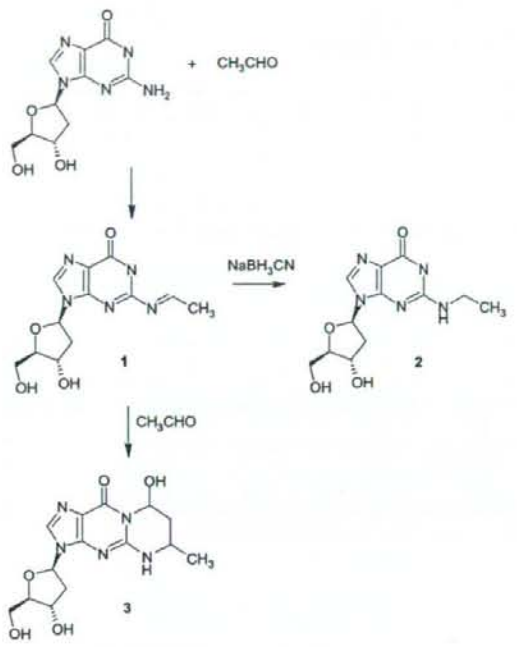

Fig. 1. Formation of acetaldehyde–deoxyguanosine adducts. **1**, N^2-ethylidene-dG; **2**, N^2-Et-dG and **3**, α-Me-γ-OH-PdG.

DNA isolation from mouse liver

For quantification of N^2-Et-dG, α-methyl-γ-hydroxy-1,N^2-propano-2′-deoxyguanosine (α-Me-γ-OH-PdG) and 1,N^6-etheno-2′-deoxyadenosine (εdA), DNA was purified from mouse liver (~50 mg amounts) by using Puregene™ DNA Purification System Cell and Tissue kit. The protocol was performed basically as described according to the manufacturer except that desferroxamine (final concentration: 0.1 mM) was added to all solutions to avoid formation of oxidative adducts during the purification step.

For quantification of N^2-ethylidene-dG, DNA was isolated from mouse liver (~50 mg amounts) as described by Wang *et al.* (15). The Puregene™ DNA Purification System Cell and Tissue kit was used. The protocol was basically as described according to the manufacturer except that $NaBH_3CN$ was added to the Puregene cell lysis solution (final concentration was 150 mM) and other solutions (2-propanol, Tris–ethylenediaminetetraacetic acid, ethanol and 70% ethanol; final concentration was 100 mM). After the purification step, DNA was dissolved in 10 mM Tris–HCl/5 mM ethylenediaminetetraacetic acid buffer (pH 7), extracted with chloroform and precipitated with ethanol also as described by Wang *et al.* (15).

DNA adduct standards and their stable isotopes

N^2-Et-dG, α-Me-γ-OH-PdG and their [U-$^{15}N_5$]-labeled standards were synthesized as described previously (14). εdA was purchased from Sigma-Aldrich Japan, Tokyo, Japan and [U-$^{15}N_5$] εdA was prepared from [U-$^{15}N_5$] dA (Cambridge Isotope Laboratory, Andover, MA, USA) following a method as described previously (17).

DNA digestion

DNA samples (20 μg) were digested to their corresponding 2′-deoxyribonucleoside-3′-monophosphates by the addition of 15 μl of 17 mM citrate plus 8 mM $CaCl_2$ buffer that contained micrococcal nuclease (22.5 U) and spleen phosphodiesterase (0.075 U) plus internal standards. Solutions were mixed and incubated for 3 h at 37°C, after which alkaline phosphatase (3 U), 10 μl of 0.5 M Tris–HCl (pH 8.5), 5 μl of 20 mM $ZnSO_4$ and 67 μl of distilled water were added and incubated further for 3 h at 37°C. The digested sample was extracted twice with methanol. The methanol fractions were evaporated to dryness, resuspended in 100 μl of distilled water and subjected to LC/MS/MS.

Instrumentation

LC/MS/MS analyses were performed using a Shimadzu LC system (Shimadzu, Kyoto, Japan) interfaced with a Quattro Ultima triple stage quadrupole MS (Waters–Micromass, Manchester, UK). The LC column was eluted over a gradient that began at a ratio of 2% methanol to 98% water and was changed to 40% methanol over a period of 40 min, changed to 80% methanol from 40 to 45 min and finally returned to the original starting conditions, 2:98, for the remaining 15 min. The total run time was 60 min. Sample injection volumes of 50 μl each were separated on a Shim-pack FC-ODS column (4.6 × 150 mm; Shimadzu) and eluted at a flow rate of 0.4 ml/min. Mass spectral analyses were carried out in positive ion mode with nitrogen as the nebulizing gas. The ion source temperature was 130°C, the desolvation gas temperature was 380°C and the cone voltage was operated at a constant 35 V. Nitrogen gas was also used as the desolvation gas (700 l/h) and cone gas (35 l/h) and argon was used as the collision gas at a collision cell pressure of 1.5×10^{-3} mbar. Positive ions were acquired in multiple reaction monitoring (MRM) mode. The MRM transitions monitored were as follows: [$^{15}N_5$]-α-Me-γ-OH-PdG, m/z 343 → 227; α-Me-γ-OH-PdG, m/z 338 → 222; [$^{15}N_5$]-N^2-Et-dG, m/z 301 → 185; N^2-Et-dG, m/z 296 → 180; [$^{15}N_5$]-εdA, m/z 281 → 165 and εdA, m/z 276 → 160. The amount of each DNA adduct was quantified by the ratio of the peak area of the target adducts and of its stable isotope. QuanLynx (version 4.0) software (Waters–Micromass) was used to create standard curves and to calculate the adduct concentrations. The amount of deoxyguanosine was monitored by a Shimadzu SPD-10A UV-Visible detector that was in place before the tandem MS.

Results

Ethanol and food intake by male mice

The male mice were fed with water or 20% ethanol and standard hard feed for 5 weeks. Feed intake was slightly decreased in the 20% ethanol group, but not significantly different between *Aldh2* genotypes. The average ethanol intake in the case of the 20% ethanol group was not significantly different between *Aldh2* genotypes (~23 g/day/kg body wt) whereas significant losses in body weight were observed only in the *Aldh2−/−* mice (data not shown).

DNA adduct levels in the liver of control and alcohol-treated mice

After 5 weeks, mice were killed and their liver DNA was purified to detect DNA adduct levels. The acetaldehyde-inducible stable DNA adducts, N^2-Et-dG and α-Me-γ-OH-PdG, were analyzed and εdA, a DNA adduct induced by lipid peroxidation, was also analyzed for comparative purposes. The LC/MS/MS instrument employed for analyzing these adducts was sensitive enough to detect at least one adduct per 10^8 bases in this experimental protocol (14). However, N^2-Et-dG was not detected in any liver DNA samples for both alcohol-treated and non-treated mice for any *Aldh2* genotype. α-Me-γ-OH-PdG and εdA were detected in all the samples analyzed but neither alcohol-dependent nor Aldh2 genotype-dependent increases in adduct levels were observed (Figure 2).

Detection of hepatic N^2-ethylidene-dG adduct in Aldh2-knockout mice

To measure N^2-ethylidene-dG in DNA, liver samples were homogenized in lysis buffer containing the strong reducing agent $NaBH_3CN$, followed by DNA purification in the presence of $NaBH_3CN$. During the purification step, it was expected that N^2-ethylidene-dG would be converted to stable N^2-Et-dG. The average N^2-ethylidene-dG level in liver DNA from untreated *Aldh2+/+* mice was 1.9 ± 0.7 adducts per 10^7 bases. Both *Aldh2* hetero- and homo-deficient genotypes did not affect N^2-ethylidene-dG levels in untreated mice. However, in the 20% ethanol-consuming mice, significant increases in the levels of N^2-ethylidene-dG in the liver DNA of *Aldh2+/+* mice (7.9 ± 1.8 adducts per 10^7 bases) and *Aldh2+/−* and *Aldh2−/−* mice were observed; levels were 23.3 ± 4.0 and 79.9 ± 14.2 adducts per 10^7 bases in *Aldh2+/−* and *Aldh2−/−* mouse liver DNA, respectively (Figure 3). These data indicated an *Aldh2* genotype-dependent increase in the levels of N^2-ethylidene-dG in liver DNA.

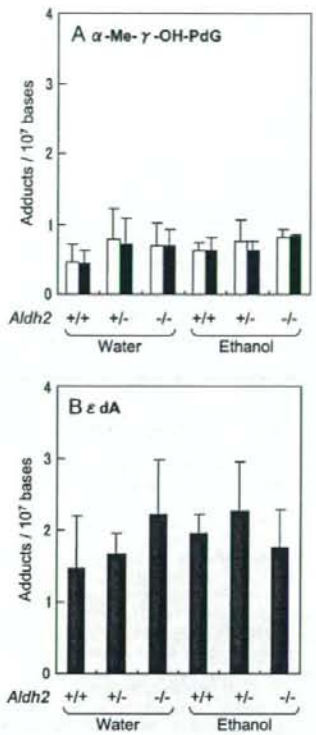

Fig. 2. DNA adduct levels in control and alcohol-treated mice having different *Aldh2* genotypes. Mice were fed with water (*Aldh2*+/+: $n = 5$, +/−: $n = 7$ and −/−: $n = 5$) or 20% ethanol (*Aldh2*+/+: $n = 6$, +/−: $n = 5$ and −/−: $n = 2$) for 5 weeks. Liver DNA samples were purified without addition of reducing agent $NaBH_3CN$. (**A**) The levels of α-Me-γ-OH-PdG (open bar: α-*S*-Me-γ-OH-PdG and closed bar: α-*R*-Me-γ-OH-PdG). (**B**) The levels of εdA. The error bars represent the standard deviation.

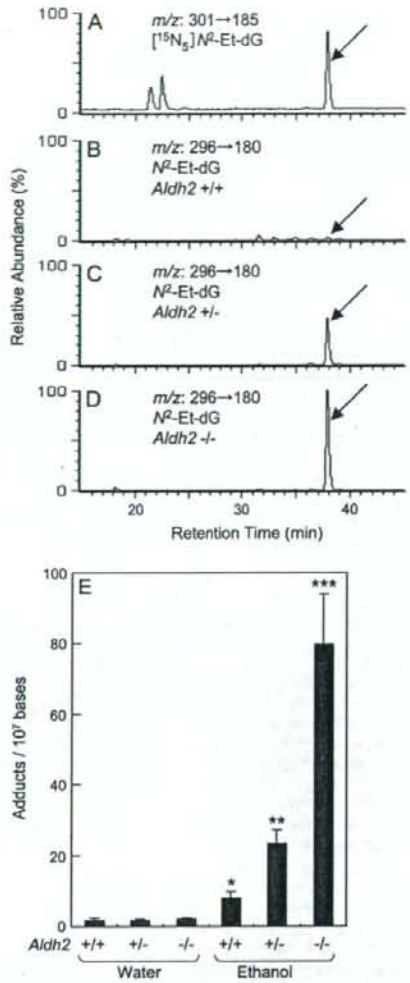

Fig. 3. Alcohol- and *Aldh2* genotype-dependent increases in N^2-ethylidene-dG levels in mice liver DNA. Mice with various *Aldh2* genotypes were fed with water (*Aldh2*+/+: $n = 5$, +/−: $n = 7$ and −/−: $n = 5$) or 20% ethanol (*Aldh2*+/+: $n = 6$, +/−: $n = 5$ and −/−: $n = 4$) for 5 weeks and the liver DNA was purified under the presence of $NaBH_3CN$ to reduce unstable N^2-ethylidene-dG to stable N^2-Et-dG. N^2-ethylidene-dG was detected as N^2-Et-dG by using LC/MS/MS. (**A**) A representative LC/MS/MS chromatogram of transition *m/z* 301 → 185 for [U-$^{15}N_5$] N^2-Et-dG as an internal standard. (**B–D**) Representative LC/MS/MS chromatograms of transition *m/z* 296 → 180 for N^2-Et-dG in *Aldh2*+/+ (**B**), +/− (**C**) and −/− (**D**) mice. (**E**) The levels of N^2-ethylidene-dG in mice liver DNA. The error bars represent the standard deviation. *Significantly increased from water control (+/+); **significantly increased from water control (+/−) or ethanol-treated *Aldh2*+/+ mice and ***significantly increased from water control (−/−) or ethanol-treated *Aldh2*+/+ and +/− mice ($P < 0.01$).

Discussion

The ALDH2-knockout mouse developed by Kitagawa *et al.* (16) has a portion of the phosphoglycerate kinase (PGK) gene promoter containing an in frame termination codon inserted immediately downstream of exon 3. The *Aldh2*−/− mouse has null mRNA of *Aldh2*, null ALDH2 protein and null mitochondrial aldehyde oxidation activity in the liver, but maintains a normal level of cytosolic aldehyde oxidation activity. In the mouse model, no ALDH2 protein is expressed from the *Aldh2*-knockout gene due to the stop codon present in the inserted PGK promoter gene. In the *Aldh2*+/− mice liver, half of the activity for metabolizing acetaldehyde remains compared with the *Aldh2*+/+ mouse. On the other hand, human *ALDH2*1/2*2* heterozygotes have only 13% of the native activity because the heterotetramers of the *ALDH2*1* and *ALDH2*2* subunits do not function properly (8). Thus, ALDH2 activity in a human *ALDH2*2/2*1* heterozygote corresponds with that of the homozygous knockout (*Aldh2*−/−) mouse rather than the heterozygous (*Aldh2*+/−) mice.

Isse *et al.* (18) reported that the blood acetaldehyde concentration after gavage of ethanol (1 g/kg body wt) of *Aldh2*−/− mice was ~18 μM and that was 9.3 times higher than that of *Aldh2*+/+ mice. Our observations show that the N^2-ethylidene-dG levels in the liver DNA of the ethanol-fed *Aldh2*−/− mice was 10 times higher than that of *Aldh2*+/+ mice, and these data are consistent with data of acetaldehyde burden. Human alcohol challenge tests have shown that after drinking a moderate amount of ethanol (0.8 g/kg body wt), the average peak in blood acetaldehyde concentrations in *ALDH2*1/2*2* individuals was 23 μM and that was 7.5 times greater than that of active *ALDH2*1/2*1* homozygotes (19). Thus, it is possible that higher

N^2-ethylidene-dG levels in liver DNA exist in drinkers having *ALDH2*1/2*2* genotypes more than in *ALDH2*1/2*1* genotypes.

On the other hand, N^2-Et-dG, a reduced product of N^2-ethylidene-dG, was not detected in any of the liver DNA samples analyzed. Since our LC/MS/MS method can detect at least one N^2-Et-dG adduct in 10^8 nucleotides, the adduct level should be at least 18–800 times lower than in the case of N^2-ethylidene-dG in mouse liver DNA. α-Me-γ-OH-PdG, another acetaldehyde-induced DNA adduct, was detected at the level of 4.5–8.1 adducts per 10^8 nucleotides, however, neither significant alcohol-dependent nor *Aldh2* genotype-dependent increases in adduct levels were observed. Previously, we determined the DNA adducts in the blood of 44 DNA samples from Japanese alcoholic patients who consumed an average of 116 g of ethanol every day for 25 years, and the levels of N^2-Et-dG and α-Me-γ-OH-PdG were significantly higher in alcoholics with the *ALDH2*1/2*2* genotype as compared with those with the *ALDH2*1/2*1* genotype (14). Since many lymphoid cells are long-lived and may persist as memory cells for several years (20), N^2-Et-dG may accumulate in the lymphoid cells of such subjects. In this study, mice were fed alcohol for only 5 weeks and that may not have been enough time for these adducts to accumulate to detectable levels in the liver, although we should consider species-specific differences and tissue-specific differences with respect to endogenous reduction of N^2-ethylidene-dG and DNA repair activity. From our data in this study at least, we can clearly say that N^2-ethylidene-dG, rather than N^2-Et-dG and α-Me-γ-OH-PdG, is a sensitive biomarker for acetaldehyde exposure *in vivo*.

There have been several studies in regard to the mutagenicity of N^2-Et-dG and α-Me-γ-OH-PdG. N^2-Et-dG adducts induce G to C mutations during DNA synthesis catalyzed by the *Escherichia coli* DNA polymerase I Klenow fragment (21) and G to T mutations during gap-filling DNA synthesis in *E.coli* cells (22). N^2-ethyl-2′-deoxyguanosine triphosphate (N^2-Et-dGTP) was effectively utilized during DNA synthesis catalyzed by mammalian DNA polymerases α and δ (23). Additionally, it has been shown that N^2-Et-dG strongly blocks replicative DNA polymerization, which leads to frameshift deletion mutations (24,25). When a single-strand shuttle vector containing a single diastereoisomer of α-Me-γ-OH-PdG was propagated in a mammalian cell line, the mutational frequency was 5–6%; G to T transversions were detected as the dominant form of damage (26). In addition, α-Me-γ-OH-PdG adducts are thought to be the precursor lesions to DNA–DNA or DNA–protein cross-links (27,28). Taken together, these observations suggest that N^2-Et-dG and α-Me-γ-OH-PdG adducts are mutagenic DNA lesions that may cause human cancers, however, in regard to N^2-ethylidene-dG, little information is yet available about its biological significance.

In closing, although the biological significance of N^2-ethylidene-dG is not clear, it was clearly shown that the adduct levels in liver DNA were relatively high and significantly increased after alcohol uptake. It will be essential to study the mutagenicity and repair properties of this sensitive and abundant alcohol- and *Aldh2* genotype-dependent biomarker in the near future.

Acknowledgements

This research was supported in part by Grants-in-aid for Cancer Research from the Ministry of Health, Labor and Welfare of Japan and Grants-in-aid for Scientific Research from the Ministry of Education, Culture, Sports, Science and Technology of Japan.

Conflict of Interest Statement: None declared.

References

1. Munaka,M. *et al.* (2003) Genetic polymorphisms of tobacco- and alcohol-related metabolizing enzymes and the risk of hepatocellular carcinoma. *J. Cancer Res. Clin. Oncol.*, **129**, 355–360.
2. Sakamoto,T. *et al.* (2006) Influence of alcohol consumption and gene polymorphisms of *ADH2* and *ALDH2* on hepatocellular carcinoma in a Japanese population. *Int. J. Cancer*, **118**, 1501–1507.
3. Bosron,W.F. *et al.* (1987) Catalytic properties of human liver alcohol dehydrogenase isoenzymes. *Enzyme*, **37**, 19–28.
4. Klyosov,A.A. *et al.* (1996) Possible role of liver cytosolic and mitochondrial aldehyde dehydrogenases in acetaldehyde metabolism. *Biochemistry*, **35**, 4445–4456.
5. Goedde,H.W. *et al.* (1992) Distribution of *ADH2* and *ALDH2* genotypes in different populations. *Hum. Genet.*, **88**, 344–346.
6. Yoshida,A. *et al.* (1991) Genetics of human alcohol-metabolizing enzymes. *Prog. Nucleic Acids Res. Mol. Biol.*, **40**, 255–287.
7. Crabb,D.W. *et al.* (1989) Genotypes for aldehyde dehydrogenase deficiency and alcohol sensitivity: the inactive *ALDH2(2)* allele is dominant. *J. Clin. Invest.*, **83**, 314–316.
8. Wang,X. *et al.* (1996) Heterotetramers of human liver mitochondrial (class 2) aldehyde dehydrogenase expressed in *Escherichia coli*. A model to study the heterotetramers expected to be found in Oriental people. *J. Biol. Chem.*, **271**, 31172–31178.
9. International Agency for Research on Cancer. (1985) Allyl compounds, aldehydes, epoxides and peroxides. *IARC Monographs on the Evaluation of the Carcinogenic Risks to Humans*, **Vol. 36.** IARC, Lyon, pp. 101–132.
10. Wang,M. *et al.* (2000) Identification of DNA adducts of acetaldehyde. *Chem. Res. Toxicol.*, **13**, 1149–1157.
11. Matsuda,T. *et al.* (1998) Specific tandem GG to TT base substitutions induced by acetaldehyde are due to intra-strand crosslinks between adjacent guanine bases. *Nucleic Acids Res.*, **26**, 1769–1774.
12. Brooks,P.J. *et al.* (2005) DNA adducts from acetaldehyde: implications for alcohol-related carcinogenesis. *Alcohol*, **35**, 187–193.
13. Fang,J.L. *et al.* (1997) Detection of DNA adducts of acetaldehyde in peripheral white blood cells of alcohol abusers. *Carcinogenesis*, **18**, 627–632.
14. Matsuda,T. *et al.* (2006) Increased DNA damage in ALDH2-deficient alcoholics. *Chem. Res. Toxicol.*, **19**, 1374–1378.
15. Wang,M. *et al.* (2006) Identification of an acetaldehyde adduct in human liver DNA and quantitation as N^2-ethyldeoxyguanosine. *Chem. Res. Toxicol.*, **19**, 319–324.
16. Kitagawa,K. *et al.* (2000) Aldehyde dehydrogenase (ALDH) 2 associates with oxidation of methoxyacetaldehyde; *in vitro* analysis with liver subcellular fraction derived from human and *Aldh2* gene targeting mouse. *FEBS Lett.*, **476**, 306–311.
17. Hillestrom,P.R. *et al.* (2004) Quantification of 1,N^6-etheno-2′-deoxyadenosine in human urine by column-switching LC/APCI-MS/MS. *Free Radic. Biol. Med.*, **36**, 1383–1392.
18. Isse,T. *et al.* (2005) Aldehyde dehydrogenase 2 gene targeting mouse lacking enzyme activity shows high acetaldehyde level in blood, brain, and liver after ethanol gavages. *Alcohol. Clin. Exp. Res.*, **29**, 1959–1964.
19. Enomoto,N. *et al.* (1991) Acetaldehyde metabolism in different aldehyde dehydrogenase-2 genotypes. *Alcohol. Clin. Exp. Res.*, **15**, 141–144.
20. Roitt,I. *et al.* (1989) *Immunology*, 2nd edn. Gower Medical Publishing, London, 2.2.
21. Terashima,I. *et al.* (2001) Miscoding potential of the N^2-ethyl-2′-deoxyguanosine DNA adduct by the exonuclease free Klenow fragment of *Escherichia coli* DNA polymerase I. *Biochemistry*, **40**, 4106–4114.
22. Upton,D.C. *et al.* (2006) Mutagenesis by exocyclic alkylamino purine adducts in *Escherichia coli*. *Mutat. Res.*, **599**, 1–10.
23. Matsuda,T. *et al.* (1999) Effective utilization of N^2-ethyl-2′-deoxyguanosine triphosphate during DNA synthesis catalyzed by mammalian replicative DNA polymerases. *Biochemistry*, **38**, 929–935.
24. Perrino,F.W. *et al.* (2003) The N^2-ethylguanine and the O^6-ethyl-and O^6-methylguanine lesions in DNA: contrasting responses form the "bypass" DNA polymerase η and the replicative DNA polymerase α. *Chem. Res. Toxicol.*, **16**, 1616–1623.
25. Upton,D.C. *et al.* (2006) Replication of N^2-ethyldeoxyguanosine DNA adducts in the human embryonic kidney cell line 293. *Chem. Res. Toxicol.*, **19**, 960–967.
26. Fernandes,P.H. *et al.* (2005) Mammalian cell mutagenesis of the DNA adducts of vinyl chloride and crotonaldehyde. *Environ. Mol. Mutagen.*, **45**, 455–459.
27. Kozekov,I.D. *et al.* (2003) DNA interchain cross-links formed by acrolein and crotonaldehyde. *J. Am. Chem. Soc.*, **125**, 50–61.
28. Kurtz,A.J. *et al.* (2003) 1, N^2-Deoxyguanosine adducts of acrolein, crotonaldehyde, and trans-4-hydroxynonenal cross-link to peptides via Schiff base linkage. *J. Biol. Chem.*, **278**, 5970–5976.

Received November 13, 2006; revised February 22, 2007; accepted March 2, 2007

Metabolic Enzyme Induction by HepG2 Cells Exposed to Oxygenated and Nonoxygenated Polycyclic Aromatic Hydrocarbons

Kentaro Misaki,[†,‡] Saburo Matsui,[‡] and Tomonari Matsuda*[,‡]

Department of Environmental Engineering and Graduate School of Global Environmental Studies, Kyoto University, Yoshidahonmachi, Kyoto 606-8501, Japan

Received August 18, 2006

Oxygenated polycyclic aromatic hydrocarbons (oxy-PAHs) such as polycyclic aromatic quinones and polycyclic aromatic ketones as well as polycyclic aromatic hydrocarbons (PAHs) are abundant in the atmospheric environment. In this study, mRNA induction of six metabolic enzymes including P4501A1, 1A2, and 1B1, aldo-keto reductase 1C1 (AKR1C1), NAD(P)H-dependent quinone oxidoreductase 1 (NQO1), and glutathione S-transferase M1 (GSTM1) were examined in detail in human hepatoma (HepG2) cells exposed to environmentally relevant 13 PAHs and seven oxy-PAHs. Most PAHs such as benzo[*a*]pyrene (B[*a*]P) showed significant induction of P4501A1 and 1A2 mRNA, while induction by oxy-PAHs such as 5,12-naphthacenequinone (NCQ) and 11*H*-benzo[*b*]fluoren-11-one (B[*b*]FO) occurred less strongly. AKR1C1 mRNA was significantly induced by oxy-PAHs, 11*H*-benzo[*a*]fluoren-11-one (B[*a*]-FO), NCQ, cyclopenta[*cd*]pyren-3(4*H*)-one (CPPO), and B[*b*]FO and also by P450s-inducing PAHs such as B[*a*]P, benzo[*k*]fluoranthene (B[*k*]FA), and dibenz[*a,h*]anthracene (DB[*a,h*]A). Both chemical-dependent and time-dependent induction patterns of NQO1 mRNA were of the mixed types of P4501A1 and AKR1C1. The tendency for the decrease of GSTM1 mRNA was observed when exposed to PAHs B[*a*]P and B[*k*]FA.

Introduction

In various atmospheric and aquatic environments, polycyclic aromatic hydrocarbons (PAHs)[1] originally derived from oil fuel and its combustion are detected at high levels (*1*−*4*), and wildlife and humans have risk of exposure. Many studies in regard to PAH mutagenicity, carcinogenicity, and DNA adduct formation have been reported (*5*−*9*). According to the U.S. Environmental Protection Agency and the International Agency for Research on Cancer (IARC), PAHs such as benzo[*a*]pyrene (B[*a*]P), benz-[*a*]anthracene (B[*a*]A), chrysene (Chr), benzo[*b*]fluoranthene (B[*b*]FA), benzo[*k*]fluoranthene (B[*k*]FA), indeno[1,2,3-*cd*]-pyrene (IdP), dibenz[*a,h*]anthracene (DB[*a,h*]A), and dibenzo-[*a,l*]pyrene were listed as probable or possible carcinogens in humans (*5*, *6*). IARC has recently changed the evaluation of several PAHs, and B[*a*]P is now classified as carcinogenic to humans (group 1) (*7*).

Oxygenated PAHs (oxy-PAHs) such as polycyclic aromatic quinones and polycyclic aromatic ketones are also present in the atmospheric environment, diesel exhaust, and airborne particles as abundant as nonoxy-PAHs (*1*−*4*); however, the toxicological significance of these compounds is not well-studied (*8*, *10*, *11*).

PAHs are considered to induce many kinds of genes such as those coding for metabolic enzymes, P450s, and phase II detoxification enzymes. The pathways for enzyme induction are especially well-known for B[*a*]P (*12*). Metabolic enzymes such as P450s are induced via the aryl hydrocarbon receptor (AhR) by B[*a*]P. AhR is present in cytoplasm as a complex with dimeric heat-shock protein 90 prior to ligand interaction. Ligands such as 2,3,7,8-tetrachlorodibenzo-*p*-dioxin (TCDD) and B[*a*]P activate AhR, and AhR transfers into the nucleus and interacts with the AhR nuclear translocator (ARNT) to form a heterodimeric transcription factor called the AhR complex, which binds xenobiotic response elements (XREs) and mediates the regulation of gene expression including specific P450s, glutathione-S-transferases (GSTs), NAD(P)H-dependent quinone oxidoreductase 1 (NQO1), growth factors, and cytokines.

B[*a*]P is metabolized to many oxygenated derivatives by P450s (*9*). Several electrophilic metabolites of B[*a*]P or reactive oxygen species (ROS) derived from them activate proteins such as activator protein 1 (AP-1) and/or the Nrf2/maf families. These activated proteins bind antioxidant response elements (AREs) or electrophilic response elements (EpREs) and enhance phase II detoxification enzymes such as aldo-keto reductases (AKRs), GSTs, NQO1, and γ-glutamylcystein synthetase (*12*−*17*).

The metabolism of B[*a*]P causes DNA damage, and three major mechanisms have been shown for the activation of DNA adduct formation by B[*a*]P. (i) A radical cation is formed

* To whom correspondence should be addressed. Tel: +81-75-753-5171. Fax: +81-75-753-3335. E-mail: matsuda@eden.env.kyoto-u.ac.jp.

† Department of Environmental Engineering.

‡ Graduate School of Global Environmental Studies.

[1] Abbreviations: PAH, polycyclic aromatic hydrocarbon; IARC, International Agency for Research on Cancer; B[*a*]P, benzo[*a*]pyrene; B[*a*]A, benz[*a*]anthracene; Chr, chrysene; B[*b*]FA, benzo[*b*]fluoranthene; B[*k*]FA, benzo[*k*]fluoranthene; IdP, indeno[1,2,3-*cd*]pyrene; DB[*a,h*]A, dibenz[*a,h*]-anthracene; oxy-PAH, oxygenated PAH; AhR, aryl hydrocarbon receptor; TCDD, 2,3,7,8-tetrachlorodibenzo-*p*-dioxin; ARNT, aryl hydrocarbon receptor nuclear translocator; XRE, xenobiotic response element; GST, glutathione-S-transferase; NQO1, NAD(P)H-dependent quinone oxidoreductase 1; ROS, reactive oxygen species; AP-1, activator protein 1; ARE, antioxidant response element; EpRE, electrophilic response element; AKR, aldo-keto reductase; B[*a*]P-7,8-diol, (±)-*trans*-7,8-dihydroxy-7,8-dihydrobenzo[*a*]-pyrene; BPDE, (±)-*trans*-7,8-dihydroxy-9,10-epoxy-7,8,9,10-tetrahydrobenzo[*a*]pyrene; BPQ, benzo[*a*]pyrene-7,8-quinone; β-NF, β-naphthoflavone; TPh, triphenylene; B[*b*]F, benzo[*b*]fluorene; 3-MC, 3-methylcholanthrene; B[*ghi*]Pe, benzo[*ghi*]perylene; N[*a*]P, naphtho[2,3-*a*]pyrene; BAQ, 7,12-benz[*a*]anthracenequinone; DB[*a,c*]A, dibenz[*a,c*]anthracene; NCQ, 5,12-naphthacenequinone; B[*a*]FO, 11*H*-benzo[*a*]fluoren-11-one; B[*b*]FO, 11*H*-benzo[*b*]fluoren-11-one; B[*c*]FO, 7*H*-benzo[*c*]fluoren-7-one; CPPO, cyclopenta[*cd*]pyren-3(4*H*)-one; BPO, 6*H*-benzo[*cd*]pyren-6-one; GAPDH, glyceraldehyde-3-phosphate dehydrogenase; IEF, induction equivalency factor.

10.1021/tx060197u CCC: $37.00
Published on Web 01/25/2007

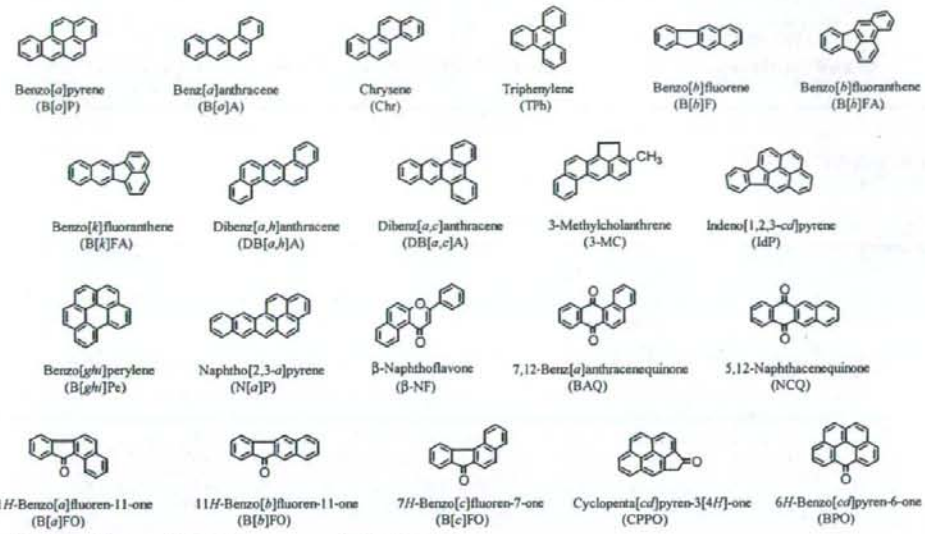

Figure 1. PAHs, oxy-PAHs, and β-NF that were examined in this study.

through a one-electron oxidation, probably via some P450s or peroxidases. This radical cation is considered to form depurinating bulky DNA adducts (*18*, *19*). (ii) B[*a*]P is metabolized to *trans*-dihydrodiols by P450s such as P4501A1 and P4501B1. One, (±)-*trans*-7,8-dihydroxy-7,8-dihydrobenzo[*a*]pyrene (B[*a*]P-7,8-diol), is then changed into a bay region diol epoxide [(±)-*trans*-7,8-dihydroxy-9,10-epoxy-7,8,9,10-tetrahydrobenzo[*a*]-pyrene (BPDE)], which forms stable and depurinating bulky DNA adducts (*9*, *19*). (iii) Suggested by Penning et al. (*12*, *13*, *20*, *21*), B[*a*]P *o*-quinone, benzo[*a*]pyrene-7,8-quinone (BPQ) is formed via AKRs. Four human AKR isoforms (AKR1C1−AKR1C4) catalyze the oxidation of B[*a*]P-7,8-diol to form a B[*a*]P catechol derivative, 7,8-dihydroxybenzo[*a*]pyrene. 7,8-Dihydroxybenzo[*a*]pyrene is then oxidized to BPQ. BPQ enters redox cycles, which are responsible for amplification of free radicals such as semiquinone anion radicals and ROS. This ROS formation is possibly related to both the initiation and the promotion stages of B[*a*]P-induced carcinogenesis (*12*, *22*−*26*).

The reports about metabolic enzyme induction of PAHs except for B[*a*]P are few (*9*, *12*, *13*, *20*, *21*, *27*−*30*). Therefore, in this study, either or both XRE (AhR) and EpRE (AP-1)-mediated typical metabolic enzyme mRNA induction levels (P450s, AKR1C1, GSTM1, and NQO1) in human hepatoma (HepG2) cells caused by 13 representative PAHs and seven oxy-PAHs were examined (Figure 1). These are representative enzymes related to the emergence of DNA adducts and detoxification.

Materials and Methods

Chemicals. TCDD was supplied by Cambridge Isotope Laboratories Inc. (Andover, MA). B[*a*]P, B[*a*]A, Chr, and β-naphthoflavone (β-NF) were supplied by Wako Chemical (Osaka, Japan). Triphenylene (TPh) and benzo[*b*]fluorene (B[*b*]F) were supplied by Tokyo Kasei Co. (Tokyo, Japan). IdP was supplied by Promochem (Wesel, Germany). The other test chemicals were supplied by Sigma-Aldrich Co. (St. Louis, MO). The purity of many test chemicals was 99−100%. The purities of B[*b*]FA, B[*k*]FA, 3-methylcholanthrene (3-MC), benzo[*ghi*]perylene (B[*ghi*]Pe), naphtho[2,3-*a*]pyrene (N[*a*]P), 7,12-benz[*a*]anthracenequinone (BAQ), and β-NF were 98%. The purities of TPh, DB[*a*,*h*]A, dibenz[*a*,*c*]-anthracene (DB[*a*,*c*]A), and 5,12-naphthacenequinone (NCQ) were 97%. The purity of B[*b*]F was 95%.

11*H*-Benzo[*a*]fluoren-11-one (B[*a*]FO), 11*H*-benzo[*b*]fluoren-11-one (B[*b*]FO), 7*H*-benzo[*c*]fluoren-7-one (B[*c*]FO), cyclopenta-[*cd*]pyren-3(4*H*)-one (CPPO), and 6*H*-benzo[*cd*]pyren-6-one (BPO) were synthesized as previously described (*31*−*34*). These compounds were purified by column chromatography and recrystallization. Only the purity of B[*c*]FO was 98%, and the purities of the other four compounds synthesized were greater than 99%.

Qiagen's RNA extraction reagent was purchased from Qiagen (Valencia, CA). Random nonamer, avian myeloblastosis virus-reverse transcriptase, and Ex Taq DNA polymerase were purchased from Takara Bio, Inc. (Otsu, Japan). Me_2SO and methanol, HPLC grade, were purchased from Wako Chemical.

HepG2 Cell Culture and RNA Isolation. The human hepatoma cell line HepG2 was obtained from the Cell Resource Center for Biomedical Research, Institute of Development, Aging and Cancer, Tohoku University, Japan. The cells were maintained in Dulbecco's modified Eagle's medium with 10% v/v fetal bovine serum (*35*). Cells were incubated at 37 °C in a humidified atmosphere containing 5% CO_2. Cells plated on 6 cm dishes were treated for 24 h with test chemicals. All chemicals were dissolved in Me_2SO, and the final concentration of the solvent in the culture medium was 0.1% v/v. Control cells were treated with 0.1% v/v Me_2SO. Total RNA was isolated from the cells using RNeasy Mini Kit (Qiagen) according to the protocol supplied by the manufacture. The RNA was dissolved in RNase free water, and the RNA concentration was determined spectrometrically. Cell cultures were conducted in triplicate for each chemical with each concentration. It was observed that HepG2 cells adhered to the dish were about half the levels in the controls when exposed to 5 μM 3-MC for 24 h. However, such extreme decreases in cell adherence were not observed until 72 h in the case of HepG2 cells that were exposed to other test chemicals.

RT and Real-Time PCR. Total RNA (100 ng) was added to a reaction mixture containing 150 ng of random nonamer, 3.5 units of AMV-RT, 25 mM Tris-HCl buffer (pH 8.3), 50 mM KCl, 2 mM $MgCl_2$, 5 mM dithiothreitol, and 1 mM deoxyribonucleoside triphosphates in a final volume of 21 μL (*35*). The reaction mixture was incubated at 37 °C for 10 min, heated at 55 °C for 30 min, and heated at 99 °C for 5 min to inactivate the enzyme.

Oligonucleotides used for PCR for four genes were commercially synthesized from Sigma Genosys Co. (Ishikari, Japan) as follows:

(i) P4501B1: 5′-TCCTGGACAAGTTCTTGAGG-3′ (508 bp) and 5′-TCAAAGTTCTCCGGGTTAGG-3′. (ii) AKR1C1: 5′-CAGGATTGGCCAAGTCCATC-3′ (256 bp) and 5′-CAAAGGACTGGGTCCTCCAA-3′. (iii) NQO1: 5′-CTGATCGTACTGGCTCACTC-3′ (202 bp) and 5′-GAACAGACTCGGCAGGATAC-3′. (iv) GSTM1: 5′-TCACAAGATCACCCAGAGCA-3′ (364 bp) and 5′-AAAGCGGGAGATGAAGTCCT-3′.

P4501A1 (433 bp), 1A2 (309 bp), and glyceraldehyde-3-phosphate dehydrogenase (GAPDH) (546 bp) primers were used from Takara's Human Cytochrome P450 Competitive RT-PCR Set. Quantification of cDNA was performed using a Smart Cycler System (Cepheid, United States), and staining was carried out with SYBR Green I. A 2 μL portion of the reverse transcriptase mixture was added to a PCR mixture containing 0.2 μM of each primer, 0.3 mM dNTPs, and 0.05 U Ex Taq DNA polymerase in a final volume of 25 μL according to Takara Ex Taq R-PCR Version 2.1 for P4501B1 gene and Version 1.0 for other genes with slight modifications. The PCR reactions were performed with Ex Taq polymerase under the following conditions (95 °C for 3 s and 65 °C for 30 s for the GAPDH and P4501A1, 1A2, and 1B1 genes; 95 °C for 3 s and 66 °C for 30 s for the AKR1C1 gene; 95 °C for 3 s and 60 °C for 30 s for the NQO1 gene; and 95 °C for 3 s and 64 °C for 30 s for the GSTM1 gene). PCR amplifications were carried out for 35 cycles for the GAPDH, P4501A1, AKR1C1, NQO1, and GSTM1 genes, for 40 cycles for the P4501A2 gene, and for 45 cycles for the P4501B1 gene. Specificity of the PCR product was determined by melting curve analysis. The expression was then normalized against the expression of GAPDH.

The concentrations producing P4501A1 mRNA equal to 25% of the maximal amount to TCDD were calculated and expressed as EC_{TCDD25}. The ratios of the EC_{TCDD25} of B[*a*]P to the EC_{TCDD25} of each of the tested compounds were calculated and were referred to as induction equivalency factors (IEFs).

Results

Induction of mRNA of Metabolic Enzymes Measured after Exposure of 5 μM PAHs and Oxy-PAHs for 24 h. The amount of P450s (P4501A1, 1A2, and 1B1), AKR1C1, NQO1, and GSTM1 mRNA in HepG2 cells induced by 5 μM of 20 representative PAHs and oxy-PAHs for 24 h was examined (Figures 2 and 3). The ratio of P4501A1 mRNA levels to GAPDH mRNA of Me_2SO control level was 1.1×10^{-2}. P4501A1 mRNA was induced by 5 μM in the case of most PAHs and some oxy-PAHs. B[*a*]P was 40-fold higher than the Me_2SO control (Figure 2A). The five-ring PAHs such as B[*k*]FA, DB[*a,h*]A, and 3-MC and the six-ring IdP were as high as or higher than the levels of induction by B[*a*]P (38- to ~58-fold). The six-ring PAH N[*a*]P induced at the highest level (80-fold) among compounds examined in this study and the four-ring PAHs B[*a*]A and Chr were slightly lower than the levels of induction by B[*a*]P (both were 29-fold). The levels of induction by four-ring oxy-PAHs, NCQ, BAQ, and B[*b*]FO and four-ring PAH and B[*b*]F were also high (21-, 17-, 15-, and 14-fold, respectively), but polycyclic aromatic ketones such as B[*a*]FO and B[*c*]FO showed low induction levels and six-ring PAH, B[*ghi*]Pe, and a representative AhR ligand, β-NF, which was used for comparison—β-NF is not an atmospheric pollutant—also showed low activities (3-, 2-, 3-, and 3-fold, respectively). The four-ring PAH, TPh, and five-ring PAK, CPPO, induced P4501A1 mRNA at the same levels as the Me_2SO control. The P4501A1 mRNA induction activity by five-ring PAK, BPO, was under half that of the control values (0.4-fold). The ratio of P4501A2 mRNA levels to GAPDH mRNA of Me_2SO control level was 8.5×10^{-4}. The tendency was observed that P4501A2 mRNA induction for test chemicals was similar to that of P4501A1 (Figure 2B). The levels of induction by B[*a*]P, B[*a*]A, Chr, B[*b*]FA, B[*k*]FA, DB[*a,h*]A, IdP, N[*a*]P, BAQ, NCQ, and

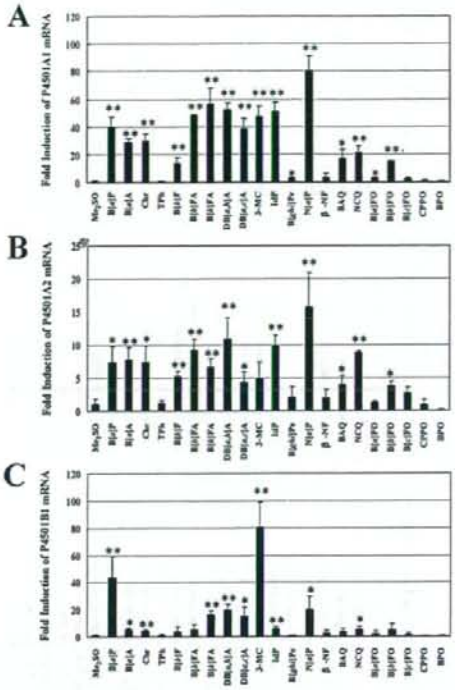

Figure 2. Induction of P450s mRNA measured by RT-PCR in HepG2 cells exposed to 5 μM PAHs and oxy-PAHs for 24 h. (A) P4501A1 mRNA, (B) P4501A2 mRNA, and (C) P4501B1 mRNA were measured. Two asterisks (**) indicate a highly significant difference from control ($p < 0.01$), and one asterisk (*) indicates a significant difference from control ($p < 0.05$) as determined by a *t*-test.

B[*b*]FO were 7-, 8-, 7-, 9-, 7-, 11-, 10-, 16-, 4-, 9-, and 4-fold, respectively. B[*c*]FO, B[*ghi*]Pe, and β-NF showed low activities (3-, 2-, and 2-fold, respectively). TPh, B[*a*]FO, and CPPO induced P4501A2 mRNA at the same levels as the Me_2SO control. The ratio of P4501B1 mRNA levels to GAPDH mRNA of Me_2SO control level was 3.5×10^{-6}. In P4501B1 mRNA induction, 3-MC was very high (80-fold) and B[*a*]P was 44-fold followed by N[*a*]P, DB[*a,h*]A, B[*k*]FA, and DB[*a,c*]A (20-, 20-, 16-, and 15-fold, respectively) (Figure 2C). B[*a*]A, Chr, B[*b*]F, B[*b*]FA, IdP, BAQ, NCQ, and B[*b*]FO were 5-, 4-, 4-, 5-, 6-, 4-, 5-, and 5-fold, respectively. The tendency was also observed that both P4501A2 and P4501B1 mRNA induced by BPO were under half that of the control values (0.1- and 0.5-fold, respectively) similar to P4501A1. The mRNA induction levels for each P450 (P4501A1, 1A2, and 1B1) by most AhR active nonoxy-PAHs were higher than AhR active oxy-PAHs at 5 μM. It was first found that 5 μM nonoxy-PAHs such as B[*b*]F, DB[*a,c*]A, and N[*a*]P and oxy-PAHs such as BAQ, NCQ, and B[*b*]FO induced CYPs.

The ratio of AKR1C1 mRNA levels to GAPDH mRNA of Me_2SO control level was 3.3×10^{-2}. AKR1C1 mRNA levels were very high in one oxy-PAH, B[*a*]FO (11-fold to Me_2SO control), and the levels are close to a representative AhR ligand and AP-1 active compound, β-NF (13-fold to Me_2SO control) (Figure 3A). B[*a*]P, B[*k*]FA, DB[*a,h*]A, NCQ, B[b]FO, and CPPO also induced AKR1C1 mRNA significantly (7-, 7-, 5-, 6-, 5-, and 5-fold, respectively).